FINAL REPORT

Innovative Nano-Encapsulated Ionic Liquid Based Surfactants for Fluorine-Free Fire Extinguishing Foams

SERDP Project WP18-1597

DECEMBER 2019

Dr. Jaspreet Dhau
Molekule, Inc.

Distribution Statement A
This document has been cleared for public release

SERDP
DOD ▪ EPA ▪ DOE

Page Intentionally Left Blank

This report was prepared under contract to the Department of Defense Strategic Environmental Research and Development Program (SERDP). The publication of this report does not indicate endorsement by the Department of Defense, nor should the contents be construed as reflecting the official policy or position of the Department of Defense. Reference herein to any specific commercial product, process, or service by trade name, trademark, manufacturer, or otherwise, does not necessarily constitute or imply its endorsement, recommendation, or favoring by the Department of Defense.

Page Intentionally Left Blank

REPORT DOCUMENTATION PAGE

Form Approved
OMB No. 0704-0188

Public reporting burden for this collection of information is estimated to average 1 hour per response, including the time for reviewing instructions, searching existing data sources, gathering and maintaining the data needed, and completing and reviewing this collection of information. Send comments regarding this burden estimate or any other aspect of this collection of information, including suggestions for reducing this burden to Department of Defense, Washington Headquarters Services, Directorate for Information Operations and Reports (0704-0188), 1215 Jefferson Davis Highway, Suite 1204, Arlington, VA 22202-4302. Respondents should be aware that notwithstanding any other provision of law, no person shall be subject to any penalty for failing to comply with a collection of information if it does not display a currently valid OMB control number. **PLEASE DO NOT RETURN YOUR FORM TO THE ABOVE ADDRESS.**

1. REPORT DATE *(DD-MM-YYYY)*
02-10-2019

2. REPORT TYPE
SERDP Final Report

3. DATES COVERED *(From - To)*
9/26/2018 - 9/26/2019

4. TITLE AND SUBTITLE
INNOVATIVE NANO-ENCAPSULATED IONIC LIQUID BASED SURFACTANTS

5a. CONTRACT NUMBER
18-P-0122

5b. GRANT NUMBER
WP18-L1-1597

5c. PROGRAM ELEMENT NUMBER

6. AUTHOR(S)
Bucchino, Matthew; Dhau, Jaspreet; Elenchin, Lena; Franz,Douglas; Maity, Krishenendu; Maximoff, Sergey

5d. PROJECT NUMBER
WP18-1597

5e. TASK NUMBER

5f. WORK UNIT NUMBER

7. PERFORMING ORGANIZATION NAME(S) AND ADDRESS(ES)
Molekule Inc.,
1301 Folsom St
San Francisco CA 94103

8. PERFORMING ORGANIZATION REPORT NUMBER
WP18-1597

9. SPONSORING / MONITORING AGENCY NAME(S) AND ADDRESS(ES)
Environmental Security Technology Certification Program
4800 Mark Center Drive, Suite 16F16
Alexandria, VA 22350-3605

10. SPONSOR/MONITOR'S ACRONYM(S)
SERDP

11. SPONSOR/MONITOR'S REPORT NUMBER(S) WP18-1597

12. DISTRIBUTION / AVAILABILITY STATEMENT
DISTRIBUTION STATEMENT A. Approved for public release: distribution unlimited.

13. SUPPLEMENTARY NOTES

14. ABSTRACT

The management of hydrocarbon fuel fires is relevant to military applications. Current firefighting formulations depend on perfluorinated surfactants. These toxic agents feature exceptionally poor biodegradability. Our objective in this proof of concept phase has been to find readily biodegradable and non-toxic firefighting formulations, which include composites of metal carbonate nanoparticles and ionic liquid surfactants. We combined experiments and computational chemistry techniques to identify those surfactants that feature high spreading coefficients over cyclohexane and bind to metal carbonate surfaces. Our experiments indicated that our formulations have spreading coefficients near or higher than the Department of Defense minimum of 3 mN/m. We also found that these surfactants form stable foams whose drainage time falls within the target range. we have demonstrated that our formulations can extinguish small scale hydrocarbon fires. Our surfactants are fluorine-free and immeasurably more biodegradable than perfluorinated surfactants that persist in the environment for decades

15. SUBJECT TERMS
Aqueous Film Forming Foam, Ionic liquids, Perfluoroalkyl surfactants, Firefighting

16. SECURITY CLASSIFICATION OF:			17. LIMITATION OF ABSTRACT	18. NUMBER OF PAGES	19a. NAME OF RESPONSIBLE PERSON
a. REPORT	b. ABSTRACT	c. THIS PAGE	SAR (Same as Report)	56	Jaspreet Dhau
UNCLASS	UNCLASS	UNCLASS			19b. TELEPHONE NUMBER *(include area code)* 813-451-5081

Standard Form 298 (Rev. 8-98)
Prescribed by ANSI Std. Z39.18

Page Intentionally Left Blank

Table of Contents

ABSTRACT 1

EXECUTIVE SUMMARY 2

OBJECTIVE 5

BACKGROUND 5

MATERIALS AND METHODS 7

SYNTHESIS OF SURFACE-ACTIVE IONIC LIQUIDS 7
CHARACTERIZATION OF SURFACE-ACTIVE IONIC LIQUIDS 10
SURFACE AND INTERFACIAL TENSION MEASUREMENTS 11
THERMOGRAVIMETRIC ANALYSIS 12
MOLECULAR DYNAMICS SIMULATIONS OF SURFACE-ACTIVE IONIC LIQUIDS 12
SURFACE AND INTERFACIAL TENSION CALCULATIONS 14
COHESIVE ENTHALPIES 14
ADSORPTION ENERGIES AT MAGNESITE AND CALCITE SURFACES FROM DENSITY FUNCTIONAL THEORY 15

RESULTS AND DISCUSSION 17

SYNTHESIS AND PERFORMANCE OF OUR FORMULATIONS 17
FIRE TESTING 22
..... 22
COMPUTATIONAL MODELING OF INTERFACIAL PROPERTIES OF AQUEOUS SOLUTIONS OF SURFACTANTS 22
MODEL VALIDATION 22
INTERFACIAL PROPERTIES OF SODIUM PERFLUOROOCTANOATE AQUEOUS SOLUTIONS. 23
INTERFACIAL PROPERTIES OF 3-ALKYL-1-METHYL IMIDAZOLIUM AQUEOUS SOLUTIONS. 26
SCREENING OVER A BROADER SET OF SURFACTANTS 32
COHESIVE ENTHALPIES AND DENSITIES. 34
ADSORPTION OF SURFACTANTS AT MAGNESITE SURFACES. 35
DESCRIPTION OF BINDING CONFIGURATIONS AT MINERAL SURFACES 35
TOXICITY AND BIODEGRADABILITY. 42

CONCLUSIONS AND IMPLICATIONS FOR FUTURE RESEARCH 43

REFERENCES 43

List of Acronyms

AFFF	Aqueous Film-Forming Foam
AFM	Atomic Force Microscopy
CMC	Critical Micelle Concentration
ChDC	Choline decanoate
DCM	Dichloromethane
DLS	Dynamic Light Scattering
DSC	Differential Scanning Calorimeter
EDS	Energy Dispersive Spectroscopy
EOR	Enhanced Oil Recovery
ESI-MS	Electrospray Ionization-Mass Spectrometry
FTIR	Fourier Transform Infrared Spectroscopy
FTS	Fluorotelomer sulfonates
GC-MS	Gas Chromatography-Mass Spectrometry
HLB	Hydrophile-Lipophile Balance
IL	Ionic Liquid
NEIL	Nanoencapsulated Ionic Liquid
NMR	Nuclear Magnetic Resonance
NP	Nanoparticle
PFAC	Perfluoroalkyl carbonates
PFAS	Perfluoroalkyl sulfonates
PFOS	Perfluorooctane sulfonate
SAIL	Surface-Active Ionic Liquid
SDBS	sodium dodecylbenzenesulfonate
SDC	Sodium decanoate
SEM	Scanning Electron Microscopy
TEM	Transmission Electron Microscopy
TGA	Thermogravimetric Analysis
UV-Vis	Ultraviolet-Visible

Keywords: Aqueous Film Forming Foam, Ionic liquids, Perfluoroalkyl surfactants, firefighting

Author contributions

Dr. Jaspreet Dhau designed the research and wrote the report.
Dr. Krishnendu Maity designed and performed synthesis, analytic measurements, and wrote the report.
Dr. Sergey Maximoff designed and performed computational simulations and wrote the report.
Dr. Douglas Franz performed density functional theory simulations and wrote the report.
Dr. Raymond Meilunas, Dr. Matthew Bucchino, and Ms. Lena Elenchin from NAVAIR designed and performed interfacial tension measurements, fire testing, and wrote the report.

Acknowledgements

We would like to thank SERDP for funding the project and giving us the opportunity to develop a non-fluorine fire-fighting foam formulation. We would also like to thank Dr. Robin Nissan and Mr. Braxton Lewis for their help on this project.

Abstract

Introduction. The management of hydrocarbon fuel fires is relevant to military applications. Current firefighting formulations depend on perfluorinated surfactants. These toxic agents feature exceptionally poor biodegradability, propagate through the food chain, and affect multiple species over an extended period. Thus, search for alternatives to perfluorinated surfactants has been assigned high priority by the U.S. Department of Defense.

Objectives. Our objective in this proof of concept phase has been to find readily biodegradable and non-toxic firefighting formulations, which include composites of metal carbonate nanoparticles and ionic liquid surfactants. These composite formulations would form stable foams and also release carbon dioxide that starves a fire of oxygen as a bonus. The ability to form stable foams that spread over hydrocarbon surface, the ability to form metal carbonate composites as well as biodegradability are key factors that we have considered in determining successful surfactant mixtures for our formulations.

Technical approach. We combined experiments and computational chemistry techniques to identify those surfactants that feature high spreading coefficients over cyclohexane and bind to metal carbonate surfaces. We used molecular dynamics simulations to predict spreading coefficients of surfactants, density functional theory to quantify the binding of surfactants to metal carbonate nanoparticle. Based on our in-silico modeling and chemical intuition, we identified, synthesized, and characterized most promising surfactant-metal carbonate composites. We then performed foam stability and small-scale fire tests.

Results. Our experiments indicated that aqueous solutions of mixtures of alkyl imidazolium or alkyl pyridinium ionic liquids as well as alkyl sulfates have spreading coefficients near or higher than the Department of Defense minimum of 3 mN/m. We also found that these surfactants form stable foams whose drainage time falls within the target range. We further established that metal carbonate nanoparticles, when added to the surfactant formulation, enhance the stability of foams. Finally, we have demonstrated that our formulations can extinguish small scale hydrocarbon fires. Our surfactants are fluorine-free and immeasurably more biodegradable than perfluorinated surfactants that persist in the environment for decades.

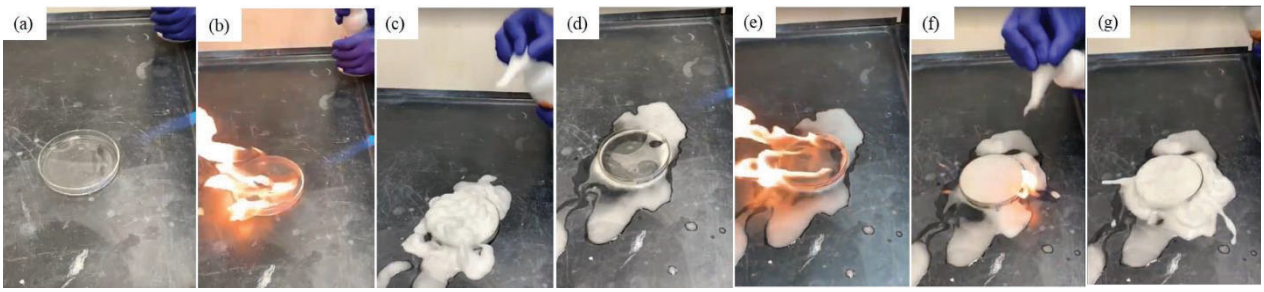

Benefits.

Our proof of concept research has provided strong evidence that ionic liquid-based formulations fully compliant with the Department of Defense standards and regulations for firefighting aqueous film-forming foams are likely achievable. Upon completion of extra work to optimize their performance, ionic liquid based formulations would mitigate risks associated with exceptionally poor biodegradability of perfluorinated surfactants currently used to extinguish jet fuel fires.

Executive Summary

Introduction

The management of hydrocarbon fuel fires is relevant to military applications. Current firefighting formulations depend on perfluorinated surfactants. These toxic agents feature exceptionally poor biodegradability. The unique film-forming property of fluorosurfactants is due to the co-existence of hydrophilic, hydrophobic, and lipophobic functionalities. The latter is not found in any other material. Therefore, we have investigated in this project an alternative out-of-the-box pathway to extinguish large hydrocarbon fires that does not rely on film-forming characteristics alone. We have developed a proof of concept formulations based on nano-encapsulated ionic liquids (NEILs), which are green chemistry agents, as alternatives to fluorinated AFFFs. Our firefighting foam formulation consists of a mixture of a long-chain surface active ionic liquid (SAIL), magnesium carbonate nanoparticles, and sodium alkyl sulfates, which are fluorine-free and biodegradable. NEIL formulations provide physical and chemical barriers that enhance the AFFF firefighting performance along multiple fronts. First, the NEIL-based formulation would form a film that seals off flammable fuel vapors. Second, the heat of the fire would trigger an endothermic reaction ($MgCO_3 \rightarrow MgO + CO_2$, $\Delta H° = 118$ kJ/mol), which generates a CO_2 blanket that smothers the fire via oxygen deprivation and fuel vapor dilution. Third, the endothermic magnesium carbonate decomposition would serve as a heat sink, and slow down endothermic foam vaporization and/or decomposition. Fourth, nanoparticles and released CO_2 would increase the foam's stability by delaying the coalescence of bubbles. Fifth, the release of IL from the core upon degradation magnesium carbonate capsules will replenish the surfactant and heal defects in the firefighting film. To our knowledge, no commercial AFFF formulations contain NEILs that have the potential to match and exceed the performance of the current AFFF formulations in use.

Objective

Any AFFF formulation that substantially decreases or eliminates these environmental risks aligns with the current priorities of SERDP. In this proof-of-concept phase, we aimed to identify formulations based on ionic liquids that meet or closely approach the requirements of the interim amendment 3 to MIL-F-24385F. A metric of success for this proof of concept phase is the number of the key requirements in the interim amendment 3 to MIL-F-24385F that our fluorine-free formulation meets or closely approach. Our ability to identify a potential roadmap to formulations that can be deployed in the real world is another metric of our success.

The requirements that a successful fluorine-free AFFF should satisfy are outlined in the interim amendment 3 to MIL-F-24385F1. The most challenging requirements that we need to address first are the following: 1) The spreading coefficient of formulation over cyclohexane should be at least 3 mN/m; 2) Foam should spread over the fuel and seal off vapor production; 3) The foam drainage time should be at least 2.5 min; 4) The burn-back resistance time should be at least 360 sec; 5) A formulation should be biodegradable, minimally toxic to aquatic life, and harmless to personnel when used as intended.

Technical approach

We combined experiments and computational chemistry techniques to identify those surfactants that feature high spreading coefficients over cyclohexane and bind to metal carbonate surfaces. We used molecular dynamics simulations to predict spreading coefficients of surfactants, and density functional theory to quantify the binding of our surfactants to metal carbonate nanoparticle. Based on our in-silico modeling and chemical intuition, we identified, synthesized, and characterized most promising surfactant-metal carbonate composites.

Results and Discussion

We have developed a successful AFFF prototype based on ionic liquids as surfactants. We have demonstrated both experimentally that a series of alkyl imidazolium-and alkyl pyridinium-based SAILs with a hydrophobic chain length of 10-12 carbon atoms work best for the reduction of water surface tension and foam stabilization. We have shown that molecular dynamics simulations can successfully predict trends in surface and interfacial tensions of aqueous solutions of surface-active ionic liquids. Density functional theory can rank different types of functional groups with respect to their ability to bind to magnesium carbonate surfaces. We have also shown using electron spray ionization mass spectrometry that ionic liquids are indeed bound to magnesium carbonate nanoparticles as intended. We performed foam stability and small-scale fire tests as a figure below illustrates.

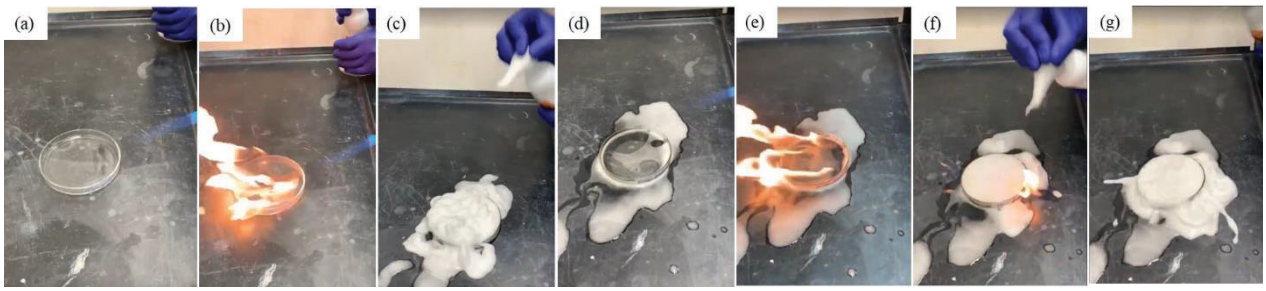

Our fluorine-free AFFF prototype formulations meet or closely approach the key requirements of MIL-F-24385F:

MIL-F-24385F requirement	**Our formulation**
spreading coefficient > 3 mn/m	as high as 3.3 mN/m
25 % drainage time > 2.5 minutes	as high as 3.9 minutes
PFOA and PFOS content < 800 ppb	fluorine-free (0)
Foam application time <45-55 s Burn back time>300-360 s	Extinguishes fire, not quantified
Fish toxicity LC_{50}(96h) for Type 3 > 500 mg/L	Estimated LC_{50} as high as 470 mg/L (N-dodecyl pyridinium) 450 mg/L (sodium dodecyl sulfate)
Biodegradability COD, BOD/CODx29	Biodegradable, not quantified
7<pH<8.5	-
Viscosity <20 centistokes at 25C Viscosity <5 centistokes at 5C	-
Refractive index > 1.3630 (Type 3)	-
Corrosion rate limits	-

Implications for Future Research and Benefits

In our future work, we will search for ionic liquids and their derivatives that have favorable interfacial properties, firefighting performance, toxicological profile, and compatibility with magnesium carbonate nanoparticles. In particular, it is known that polar groups in the alkyl chains or a change in head groups of ionic liquids can significantly lower the toxicity. The initial screening

effort can be accomplished with computational chemistry screening tools, which can be used to predict both toxicity and interfacial properties. Successful formulations identified in *in silico* screening can be further examined experimentally. The costs of *in silico* materials design efforts are significantly lower than those for actual experiments. In this phase, we did not attempt to optimize refractive index, viscosity, pH, and corrosion rate, but we plan to address these factors in the next phase by adding components that do not impact the firefighting performance. Upon completion of the follow up research to optimize their performance, formulations based on ionic liquids would mitigate risks associated with exceptionally poor biodegradability of perfluorinated surfactants currently used to extinguish jet fuel fires.

Objective

Nonbiodegradable fluorinated aqueous film-forming foam (AFFF) formulations persist in the environment for decades, propagate all the way from the bottom to the top of the food chain, and cause adverse effects on various organisms. Any AFFF formulation that substantially decreases or eliminates these environmental risks aligns with the current priorities of SERDP. To replace eco-toxic and nonbiodegradable fluorinated AFFF in fire-suppression operations, we proposed to develop innovative and cost-effective fluorine-free formulations containing metal carbonate nanoencapsulated ionic liquid surfactants. In this proof-of-concept phase, we aimed to identify formulations based on nanoencapsulated ionic liquids that meet or closely approach the requirements of MIL-F-24385F[1]. A metric of success for this proof of concept phase is the number of the key requirements in MIL-F-24385F[1] that our fluorine-free formulation meets or closely approach. Our ability to identify a potential roadmap to formulations that can be deployed in the real world is another metric of our success.

Background

Aqueous film-forming foams (AFFF) have numerous applications in industry and defense sectors. AFFFs are used predominantly as fire-fighting retardants that actively extinguish hydrocarbon fires. It is a well- developed technology used by the US Department of Defense since the early 70's[2]. AFFF's are known for their ability to extinguish fires rapidly and effectively, long shelf-life, self-healing ability, compatibility, and ease in handling[3]. Film drainage or break-ups, coalescence, and disproportionation effects[4, 5] in AFFFs have been extensively studied[6-10]. Until now, the AFFFs made of fluorinated surfactants have demonstrated superior firefighting performance capabilities because of the co-existence of hydrophilic, hydrophobic and lipophobic head groups. The latter properties are responsible for creating a thin film that seals off the surface of burning hydrocarbon fuels[11-13]. However, the inherent toxicity and exceptionally poor biodegradability of the fluorochemicals, including perfluoroalkyl carbonates (PFAC), perfluoroalkyl sulfonates (PFOS) and fluorotelomer sulfonates (FTS), are a significant threat to the environment[14]. Thus, a fluorine-free disruptive technology is urgently needed[15].

Fluorine-free foams from two different manufacturers (Angus Fire Armour and 3M) have been tested using dynamic surface and interfacial tension. These fluorine-free foams do not produce a thin-film blanket over the burning fuel as required by MIL-F-24385F[1]. Similarly, foam degradation has been tested for both fluorinated and nonfluorinated (or fluorine-free) foams[16]. These fluorine-free foams exhibited faster degradation when compared to AFFFs. Another alternative approach to producing non-aqueous foams with specialty surfactants (PoliDiMethylSiloxane, PDMS), solid and/or crystalline particles as stabilizers are emerging technologies in petroleum and food industries[17].

The unique film-forming property of fluorosurfactants is due to the co-existence of hydrophilic, hydrophobic, and lipophobic functionalities. The latter is not found in any other material. Therefore, we have investigated in this project an alternative out-of-the-box pathway to extinguish large hydrocarbon fires that does not rely on film-forming characteristics alone. We have developed a proof of concept formulations based on nano-encapsulated ionic liquids (NEILs),

which are green chemistry agents[18-21], as alternatives to fluorinated AFFFs. Our firefighting foam formulation consists of a mixture of a long-chain surface active ionic liquid (SAIL), magnesium carbonate nanoparticles, and sodium alkyl sulfates, which are fluorine-free and biodegradable.

NEIL formulations provide physical and chemical barriers that enhance the AFFF firefighting performance along multiple fronts. First, the NEIL-based formulation would form a film that seals off flammable fuel vapors. Second, the heat of the fire would trigger an endothermic reaction ($MgCO_3 \rightarrow MgO + CO_2$, $\Delta H° = 118$ kJ/mol), which generates a CO_2 blanket that smothers the fire via oxygen deprivation and fuel vapor dilution. Third, the endothermic magnesium carbonate decomposition would serve as a heat sink, and slow down endothermic foam vaporization and/or decomposition. Fourth, nanoparticles and released CO_2 would increase the foam's stability by delaying the coalescence of bubbles. Fifth, the release of IL from the core upon degradation magnesium carbonate capsules will replenish the surfactant and heal defects in the firefighting film. To our knowledge, no commercial AFFF formulations contain NEILs that have the potential to match and exceed the performance of the current AFFF formulations in use.

Table 1. *A summary of MIL-F-24385F requirements and the performance of our formulations.*

MIL-F-24385F requirement	**Our formulation**
spreading coefficient > 3 mn/m	as high as 3.3 mN/m
25 % drainage time > 2.5 minutes	as high as 3.9 minutes
PFOA and PFOS content < 800 ppb	fluorine-free (0)
Foam application time <45-55 s Burn back time>300-360 s	Extinguishes fire, not quantified
Fish toxicity LC_{50}(96h) for Type 3 > 500 mg/L	Estimated LC_{50} as high as 470 mg/L (N-dodecyl pyridinium) 450 mg/L (sodium dodecyl sulfate)
Biodegradability COD, BOD/CODx29	Biodegradable, not quantified
7<pH<8.5	-
Viscosity <20 centistokes at 25C Viscosity <5 centistokes at 5C	-
Refractive index > 1.3630 (Type 3)	-
Corrosion rate limits	-

The requirements that a successful fluorine-free AFFF should satisfy are outlined in the interim amendment 3 to MIL-F-24385F[1]. The most challenging requirements that we need to address first are the following: 1) The spreading coefficient of formulation over cyclohexane should be at least 3 mN/m; 2) Foam should spread over the fuel and seal off vapor production; 3) The foam drainage time should be at least 2.5 min; 4) The burn-back resistance time should be at least 360 sec; 5) A formulation should be biodegradable, minimally toxic to aquatic life, and harmless to personnel when used as intended. For our prototypes of ionic liquid-based formulations, we have addressed the points 1-4 experimentally. We also investigated the point 1 using computational models. The point 5 has been addressed on the basis of existing literature. In addition to these requirements, we need to investigate the compatibility of our surfactants and encapsulating magnesium carbonate nanoparticles. We have demonstrated in this proof of concept project that fluorine-free formulations containing alkyl imidazolium or alkyl pyridinium ionic liquids and sodium dodecyl

sulfate are able to satisfy or closely approach the key requirements of MIL-F-24385F[1]. That said, we have only scratched the surface with this limited scope project. We have found a strong evidence to pursue ILs as a potential substitute of PFAS, however a sustained effort is required to further improve the formulation and test its efficacy in extinguishing large fires. Specific requirements of MIL-F-24385F[1] that we have addressed in this project are summarized in Table 1.

Materials and Methods

Synthesis of surface-active ionic liquids

We have synthesized a series of imidazolium and pyridinium based ionic liquids having tail lengths 10 to 18 C-atoms long. The syntheses of SAILs required just one step under solvent-free conditions and the starting materials were very cheap and readily available from commercial suppliers. This is crucial to ensure scalability of the synthetic methodologies to produce ILs on a large scale.

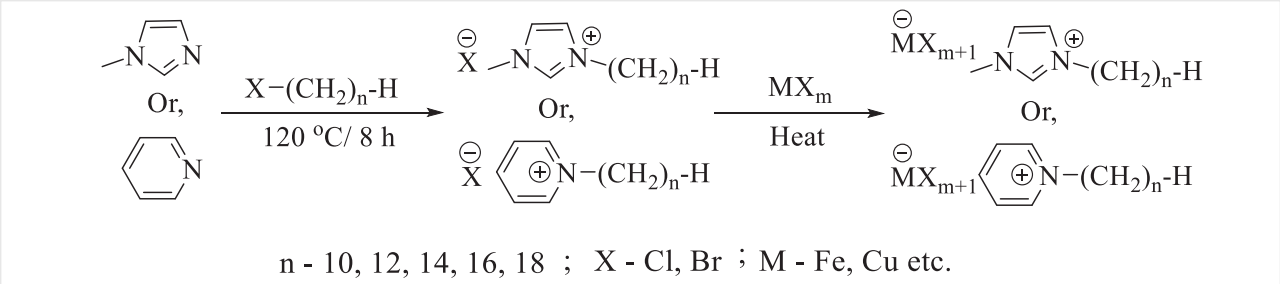

Scheme 1: Synthesis of cationic-IL surfactants and metallosurfactants

SAILs/surfactants with positive head-groups such as alkylimidazolium, alkylpyridinium and ammonium; negative head-groups such as alkylsulfonate, alkylsulfate and carboxylate; zwitterionic head-groups such as betaines, sulfobetaines and pyridine N-oxides were synthesized and mixed in different proportions during the screening process. Imidazolium and pyridinium based SAILs were synthesized by heating a mixture of alkyl halides with 1-methylimidazole and pyridine respectively at 120 ºC for 8 hours[22, 23]. Upon cooling the reaction mixture got solidified and the crude products were recrystallized from ethylacetate/ hexane (90:10) mixture. The corresponding metallosurfactants were synthesized by heating a mixture of the IL and either $CuCl_2$ or $FeCl_2$ at 100 ºC for 4 hours[24, 25].

Anionic SAILs were synthesized via salt metathesis as depicted in scheme below[26]. Clear solutions of the sodium salts of alkyl sulfate, sulfonate and carboxylates, and choline chloride in MeOH

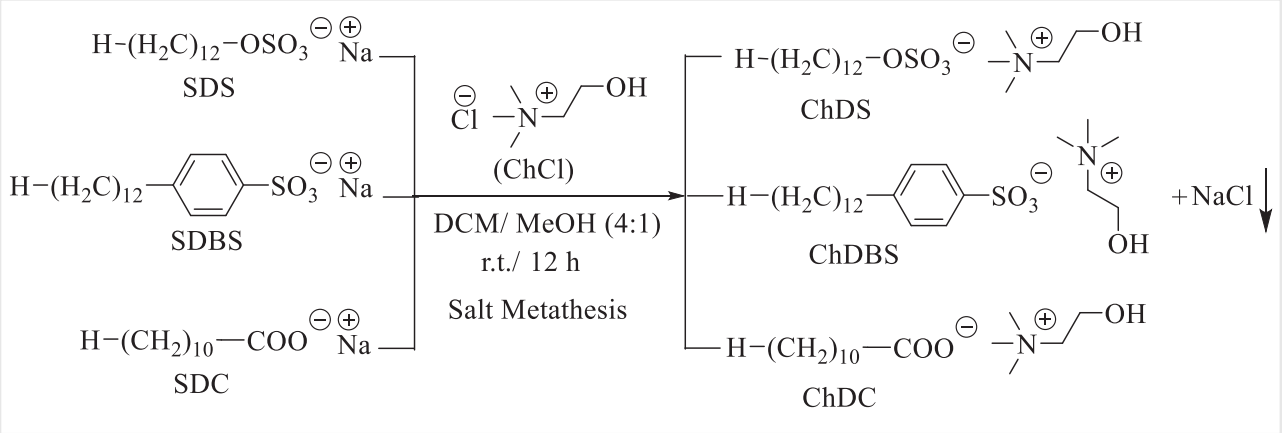

Scheme 2: Synthesis of anionic-IL surfactants via salt metathesis metathesis

were prepared separately and mixed together at room temperature. The mixture was then diluted four times with dichloromethane (DCM). The precipitated NaCl was filtered off and the solvents were evaporated under vacuum to yield white waxy products. The absence of NaCl in the final products were confirmed by $AgNO_3$ test.

The betaine and sulfobetaine[27-29] zwitterionic liquid (ZIL) surfactants were synthesized following literature reported procedure. As expressed in scheme below, an equimolar mixture of different

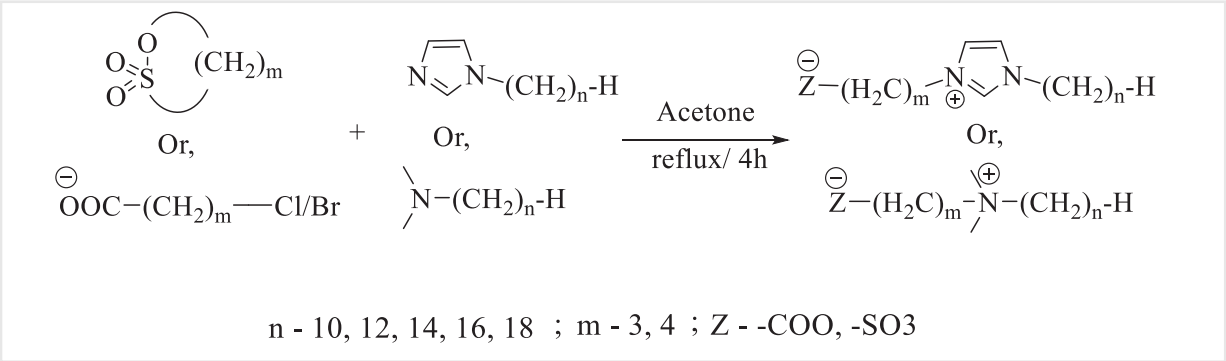

Scheme 3: Synthesis of Zwitterionic-IL Surfactants

combinations of long chain alkylimidazole or tertiary amine, and alkane-sultone or halo-carboxylate were heated under reflux in acetone for 4 hours to furnish the corresponding ZILs. The crude products were recrystallized from MeOH.

We have synthesized polymer ILs (PILs) displayed in schemes below, and plan to use them as additives in our formulations as foam stabilizer as well as rheology modifier.

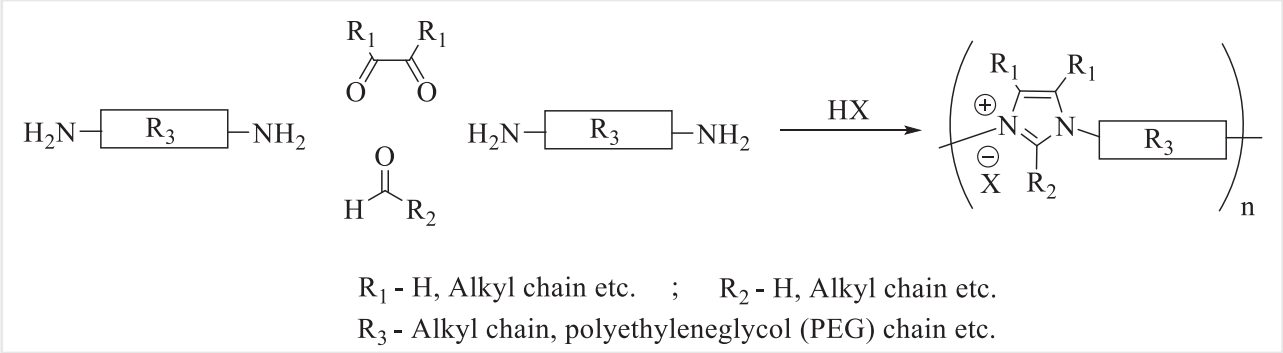

Scheme 4: Polymer ionic liquid (PIL) synthesis via Radziszewski reaction[30]

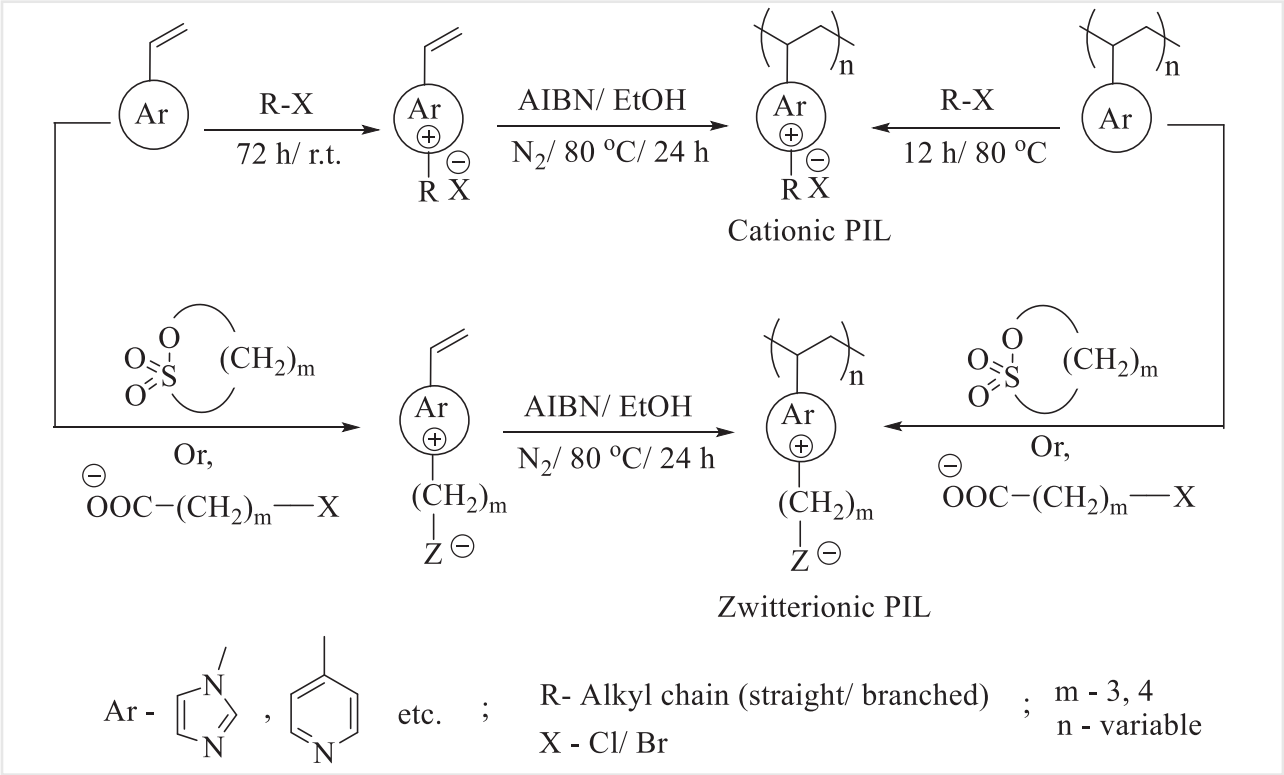

Scheme 5: Polymer ionic liquid synthesis via radical polymerization[31]

The effect of carbonate nanoparticles on foam stability was assessed. $CaCO_3$ nanoparticles were prepared by both top-down physical and bottom-up solution method. In the top-down physical ball-milling method, a 1:1:3 mixture of $CaCl_2$:Na_2CO_3:NaCl was pulverized for 2 hours at 300 rpm, with 1:40 mass ratio of the sample and the balls weighing 4 gm each. NaCl was used as a diluting agent to control the size of the nanoparticles. In the solution method, a 100 ml 0.1 M solution of Na_2CO_3 and C_1C_{10}ImCl was added dropwise to a solution of 100 ml 0.1 M $CaCl_2$ and sodium dodecylbenzenesulfonate (SDBS) in water. The nanoparticles were centrifuged and washed thoroughly before use. $MgCO_3$ NPs were synthesized following similar method to that of

$CaCO_3$ NPs. Having control over the reaction conditions and outcomes were proven difficult in case of $MgCO_3$ NPs.

Synthesis of the NEIL-1 (encapsulated 1-dodecyl-3-methylimidazolium chloride IL liquid in $CaCO_3$ shells with the help of Brij S20 co-surfactant) was achieved by following a similar procedure reported in literature. Firstly, an equimolar mixture of $C_1C_{10}ImCl$ (0.5 mmol) and Brij S-20 (0.5 mmol) was stirred in water (10 ml) for 2 hours at room temperature. Then a solution of $CaCl_2$ (1 mmol) in water (2 ml) was added at once followed by the dropwise addition of a solution of Na_2CO_3 (1 mmol) in water (2 ml). The resulting milky solution was kept on stirring for 12 hours at room temperature. Thereafter the white suspension was centrifuged to separate the white nano capsules. The NEILs were washed several times with distilled water to get rid of any leftover surfactants attached to the outer surface of the capsules. Although similar approach was followed to fabricate $MgCO_3$ shell, no core-shell structure was apparent in the TEM micrographs.

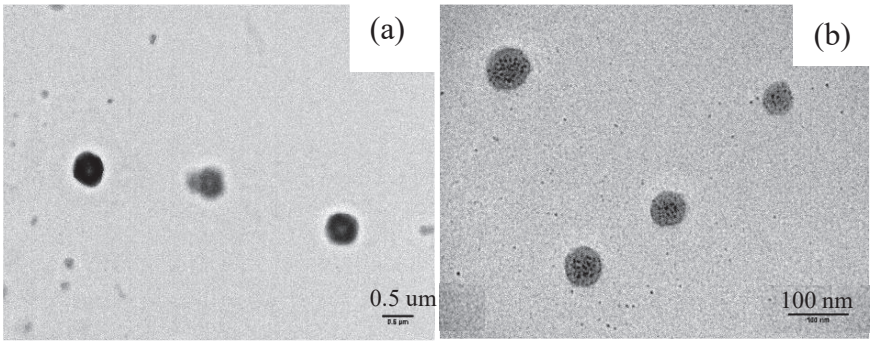

Figure 1. *(a) NEIL-1; scale bar is 0.5 µm, (b) $MgCO_3$ NPs; scale bar is 100 nm.*

Characterization of surface-active ionic liquids

All the synthesized SAILs/surfactants were characterized by NMR and mass spectrometry and matched with the literature before proceeding further. Thermo gravimetric analyses (TGA) were carried out on a TGA Q50 instrument. TGA provided us with the information about the thermal stability, decomposition/evaporation temperature of the SAILs, surfactants and NEILs. SAILs/surfactants with higher decomposition temperature are desirable. Differential scanning calorimetry (DSC) analyses were performed on a DSC Q20 instrument to reveal the enthalpy of vaporization, onset of degradation etc. and help us understand the effect of the nanoencapsulation of the ILs relative to free ILs. The surface modification of the NEILs by ILs was studied via ATR-FTIR. Transmission electron microscopy (TEM) studies were carried out to confirm the core-shell structure of the NEILs. Size distribution of the NEILs and the neat carbonate nanoparticles were studied using dynamic light scattering (DLS) in Zetasizer Nano-ZS instrument. The surface tension studies were carried out via pendant drop technique using KSV CAM-101 instrument. In this optical technique, the curvature of the pendant liquid drop from a needle is analyzed by a software. DuNuoy ring tensiometer was used to carry out both surface tension and interfacial tension studies. For

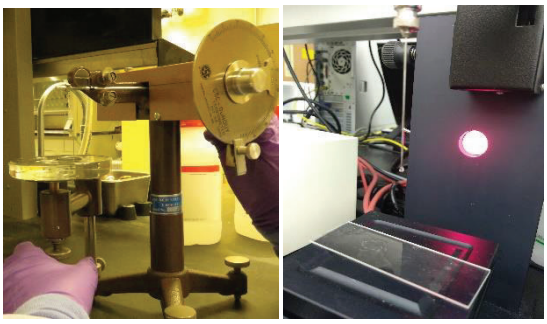

Figure 2. *Surface tension and interfacial tension were measured by (a) DuNouy ring and (b) pendant drop methods.*

foamability, foam stability and foam drainage testing, we used an air aspirating foam dispenser and weight-fall method. A surfactant solution of known concentration was used to generate foam inside a graduated burette. The water drained out of the column was collected in a graduated measuring cylinder and a plot of vol of water drained vs time was generated. As water drained out, the foam column height gradually decreased and eventually vanished. The total volume of water that drained out of the column was recorded. A 25% foam drainage time was then calculated from the plot by measuring the time it took to drain out 25% of the total drained water. Foam expansion ratio was calculated by dividing the initial foam volume by the volume of total drained water. We have developed a new method, namely weight-fall method, to check the stability and strength of the foam column. In this method we suspend a loosely fitted disc of appropriate weight on top of the foam column and monitor the descent of the disc over time. With the drainage of the liquid from the foam column, the upper lamellas get thinner and eventually gets destroyed by the weight, thereby providing us with a true measurement of the foam height that is thick enough to serve the purpose. The advantage of weight-fall method is that it is quick and requires relatively less amount of surfactant. Therefore, multiple experiments can be done to achieve a statistically accurate result.

Surface and interfacial tension measurements

A DuNouy Ring Precision Tensiometer (CSC Scientific Company, Inc.) in Figure 3 was implemented to test foam film-forming capability. Surface and interfacial tensions of Navy qualified 3% AFFF concentrates versus the numerous ionic liquid mixtures IAW MIL-PRF-24385 (4.7.4.1 and 4.7.4.2) and ASTM D1331 (Standard Test Methods for Surface and Interfacial Tension of Solutions of Paints, Solvents, Solutions of Surface-Active Agents, and Related Materials) were measured. Typical surface/interfacial tension readings have a precision of approximately +/- 0.1 Dynes/cm. A platinum ring (R/r = 51.155, mean circumference = 6.09 cm, Serial #: 110118887) with a water contact angle near zero was used as the torsional wire to measure the force necessary to detach (i.e. break the meniscus) from the foam surface (or foam / fuel interface). All measurements were performed at room temperature. Interfacial tension experiments were conducted between the foam concentrates and reagent grade cyclohexane as specified in MIL-PRF-24385, with the platinum ring moving from the foam (i.e. aqueous side) of the interface through to the cyclohexane (i.e. non-aqueous) side. The platinum ring was thoroughly washed with solvent and rinsed with distilled water after each test. Foams were allowed to rest 2-3 minutes after the foam/cyclohexane interface was established in order to ensure the readings came in to equilibrium and could be correlated to theoretical calculations. Figure 3 below displays a representative cyclohexane (top layer) / foam (bottom layer) interfacial tension measurement. This photograph was collected just prior to the meniscus break.

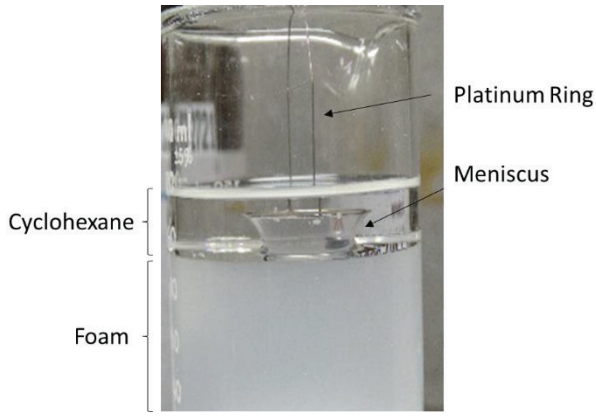

Figure 3. *Interfacial tension measurement using the DuNouy Ring Precision Tensiometer.*

Thermogravimetric analysis

A TA Instruments Discovery Series Thermograviemtric Analyzer (TGA) connected to a single quadrupole mass spectrometer (via a heated transfer line) was used to identify gaseous products released from the ionic liquids and to assess their rate of thermal degradation. Experiments were primarily conducted in a nitrogen atmosphere with temperature ramp profiles from 30C to 600C (@ 20C/minute). Metal carbonates absorb the heat (i.e. from fire) via an endothermic reaction, which can prevent foam collapse/evaporation and generate a carbon dioxide blanket to smother fire via oxygen deprivation. This hyphenated analytical technique tracked relative amounts of CO_2 released from the metal carbonate encapsulated ionic liquids as a function of temperature.

A TA Instruments Discovery Series Simultaneous Differential scanning calorimeter / Thermogravimetric (SDT 650) was used to assess the simultaneous heat flow and weight loss of the encapsulated ionic liquids. Advantages of this particular instrument versus standalone DSC and TGA techniques is the ceramic furnace that permits temperature measurements from ambient to 1,500C. The measured enthalpy of vaporizations were used to down select the encapsulated ionic liquid based on the kinetic barrier to vaporization imposed by the encapsulation.

Molecular dynamics simulations of surface-active ionic liquids

To model surface and interfacial tensions of our surfactants, we employed molecular dynamics simulations. Molecular dynamics simulations can successfully predict both the surface and interfacial tension if an appropriate force field is used. In particular, surfaces of pure liquids[32] and surfactants adsorbed at liquid interfaces[33-40] have been modeled using molecular dynamics or dissipative particle dynamics. Dissipative particle dynamics models that give quantitative predictions for interfacial properties of ionic surfactants are difficult to design. Therefore, we relied on molecular dynamics models.

We performed molecular dynamics simulations to compute surface tensions, interfacial tensions and spreading coefficients of aqueous solutions of ionic liquids and other surfactants as well as enthalpies of vaporization of surface-active ionic liquids. In our molecular dynamics simulations, we used the general amber force field (GAFF)[41], which was trained to describe properties of a broad range of organic compounds. This approximation was validated for predicting densities,

surface tensions, and enthalpies of vaporization of a variety of organic liquids[42]. It also was specifically validated for densities and enthalpies of vaporizations of ionic liquids[43]. To describe water, we relied on the TIP4P/2005[44], which is a successful model for a variety of properties, including the surface tension[45]. We used force field parameters for small anions and cations derived by Merz group[46, 47]. The real space cut off for the Lennard-Jones potential was set to 0.12 nm. No tail correction was used. The Coulomb interaction was computed using the particle-particle-particle-mesh method with 0.12 nm radius used for delimiting the real and reciprocal space contributions to the Coulomb interaction. Bonds shorter than 0.11 nm were constrained to their equilibrium lengths by the SHAKE constraint in all our molecular dynamics simulations to afford longer integration time step. The latter was set to 2 fs. We used the Nose-Hoover thermostat and Parinello-Rahman barostat to control the temperature and pressure in the NVT and NPT simulations.

Adsorption of surfactant molecules or ions at interface occurs at a time scale that is hard to access in a molecular dynamics simulation directly. Therefore, we prebuild initial configurations of a pair parallel planar monolayers (Figure 4) using a Monte Carlo algorithm as implemented in PackMol[48]. Surfactant molecules in a monolayer at a given surface coverage were placed nearly perpendicular to the interface with hydrophilic ends facing the aqueous phase. The aqueous phase between the monolayers contains 8000 water molecules. The initial unit cell in the plane of the monolayers is square with the side about 5 nm (Figure 4B). The dimension of the water box orthogonal to the monolayer planes is about 10 nm. To create an aqueous solution-vapor interface, the unit cell was elongated in the direction orthogonal to the surfactant monolayer so that the long dimension of the unit cell is 53.2 nm (Figure 4B).

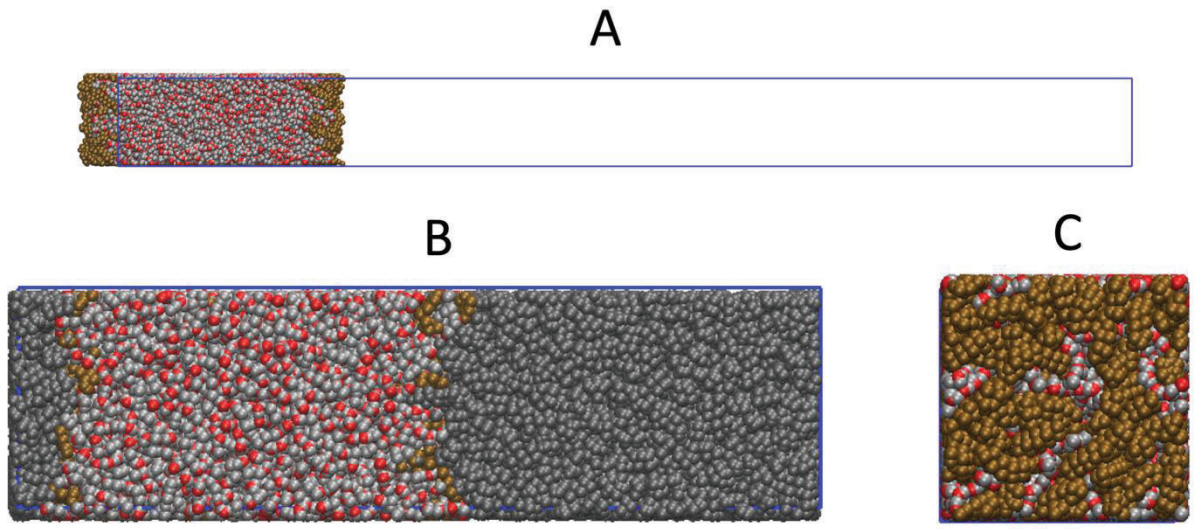

Figure 4. *A unit cell used in surface tension (A) and interfacial tension (B) calculations. Silver and red spheres are water's hydrogen and oxygen atoms, respectively. Ochre spheres are surfactant's atoms. Cyclohexane atoms are shown in dark gray. A view of the simulation cell from atop (C).*

To equilibrate the system, we minimized the total energy of the constructed system with respect to atom coordinates and then performed an NPT molecular dynamics simulation at 298 K and 1 bar for 3 ns with the volume fluctuations driven by changes in X and Y directions parallel to the monolayer. Planar harmonic wall constraints were imposed just above the ends of the surfactant molecules in the initial configuration to prevent changes in the dimensions of the film in the Z direction. Then the harmonic wall constraints were removed, and the system was let to equilibrate in the NVT ensemble for another 3 ns.

To create an initial configuration of aqueous solution-hydrocarbon interface, we followed our procedure for generating aqueous solution-vapor interface, and then filled the vacuum slab of about 10 nm thick with cyclohexane molecules at the experimental density. The total energy of the constructed system was then minimized with respect to atom coordinates. To equilibrate the system, we performed NPT molecular dynamics simulations at 298 K and 1 bar for 3 ns with the volume fluctuations driven by changes in Z direction only to prevent large changes in surfactant surface coverage. Then the system was left to equilibrate in the NVT ensemble for another 3 ns.

Surface and interfacial tension calculations

To estimate the surface or interfacial tensions at a given surfactant surface coverage, we continued the NVT molecular dynamics simulation after the equilibration for another 10 ns while sampling the local pressure tensor along Z direction by binning the simulation unit cell into 0.3 nm thick slabs orthogonal to the Z direction. The surface or interfacial tension is then given by the anisotropy of the local pressure tensor along Z:

$$\gamma = \frac{1}{2}\int\left(P_{ZZ}(z) - \frac{1}{2}(P_{XX}(z) + P_{YY}(z))\right)dz. \qquad (1)$$

The surface or interfacial tension can alternatively be computed as

$$\gamma' = \langle P_t \rangle - \langle P_n \rangle, \qquad (2)$$

where $\langle P_t \rangle$ and $\langle P_n \rangle$ are the time averages of components of the global pressure tensor in the directions tangential and normal to the interface, respectively. Eqs. (1) and (2) may result in slightly different numbers in a simulation of finite duration. As a non-polarizable force, GAFF field tends to underestimate experimental surface tensions in average[42]. Since adsorption isotherms for surfactants are not available to us, we computed surface tension as a function of surfactant surface coverage. We computed the spreading coefficient as

$$S_{cyclohexane/surfactant} = \gamma_{cyclohexane} - \left(\gamma_{surfactant} + \gamma_{surf,cyclohexane}\right). \qquad (3)$$

Cohesive enthalpies

To compute the bulk properties of ionic liquid surfactants, we placed 750 randomly distributed ion pairs in a cubic box at an initial density of 1 g/cm^3. Then the total energy of the system was minimized with respect to the atomic coordinates, and the system was equilibrated in the NPT ensemble for 6 ns. The last 3 ns were used to compute the average density and enthalpy H_{liquid}. The cohesive enthalpy is given by

$$\Delta H_{cohesive} = H_{liquid} - N(RT + E_{ion\,pair}). \qquad (4)$$

Adsorption energies at magnesite and calcite surfaces from density functional theory

A 4-layer (10.4) magnesite ($MgCO_3$) surfaces were cleaved using Materials Studio from the experimental crystal structures[49, 50]. The (10.4) surface is known to be the most stable and common for calcite and magnesite[51, 52]. The slab was built as a 1x2 supercell. A single layer of water molecules was placed along the surface at a 1 H_2O/Mg ratio with the O_{H2O}...Mg axis perpendicular to the plane of the surface (as in the regular herringbone pattern), followed by the molecule of interest, followed by another 4 layers of H_2O above the molecule. Thus, the total system in each case featured 80 atoms from the magnesite slab, 20 H_2O molecules (or 60 atoms), and the molecule of interest in between the two water layers to simulate solvation near the surface. An example of this setup is shown in Figure 5.

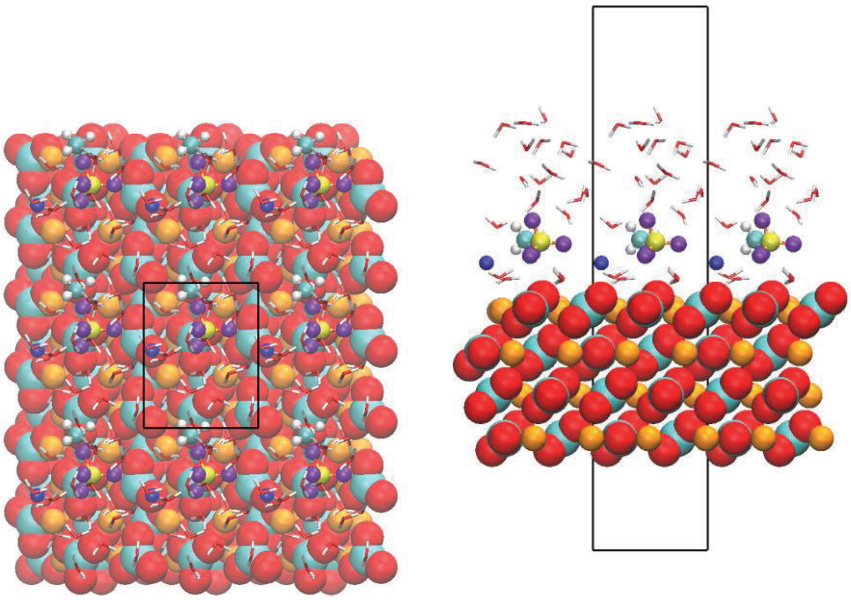

***Figure 5**. A sample configuration of magnesite (bottom layers) with sodium methylsulfate in aqueous solution. Atom colors are C: cyan; O: red; H: white; Mg: pink; Na: blue; S: yellow. Sulfate oxygens are shown in purple. The bounding periodic box is shown with blue lines.*

We performed our periodic DFT calculations using the PBE functional subject to the DFTD3 dispersion correction as implemented in CP2K[53]. The cut-off radius for the dispersion correction was set to 6.09Å. The periodic boundary conditions were applied in the directions coplanar with the slab surface. The reciprocal space quadratures were evaluated at the Γ point. We verified that the inclusion of more k-points in the quadratures did not significantly alter adsorption energies. Each system of interest was optimized fully while constraining the periodic box parameters and the coordinates of the bottom 2 layers of in the magnesite slab. The optimizations were considered converged when the maximum step size was $\leq 6.0\text{x}10^{-3}$, the RMS step size was $\leq 1.5\text{x}10^{-3}$, the maximum gradient was $\leq 4.5\text{x}10^{-4}$, and the RMS gradient was $\leq 3.0\text{x}10^{-4}$. The Kohn-Sham equations were solved using direct energy minimization with the conjugate gradient method as implemented in CP2K[53]. Each optimization step SCF convergence was achieved when the total energy changed by less than $5.0\text{x}10^{-7}$ Hartree. We used gaussian basis functions to represent the

Kohn-Sham orbitals. The electron density was expanded over plane waves. The core electrons were described by the GTH-PBE-q pseudopotentials[53]. The DZVP-MOLOPT-GTH basis sets were used for all atoms except Na, S, Mg, which were treated with DZVP-MOLOPT-SR-GTH basis sets as implemented in CP2K[53].

The binding energies of molecules to the calcite reported here are computed from the final optimized configuration as

$E_{all} - E_{H2O} - E_{mol} - E_{slab} - E_{bind,\ mol/H2O} - E_{bind,\ H2O/slab}$,

i.e., the total binding energy $E_{all} - E_{H2O} - E_{mol} - E_{slab}$ with the binding of hydration of the molecule and binding of water to the slab subtracted off. A shortened expression for this energy is
$E_{bind,\ mol/slab} = E_{all} - E_{mol+H2O} - E_{H2O+slab} + E_{H2O}$.

Results and Discussion

Synthesis and performance of our formulations

We have synthesized and screened a series of SAILs and found that a hydrophobic chain length of 10-12 carbon atoms work best for the reduction of the surface tension of water and foam stabilization. Increase in the vaporization temperatures and melting points with increasing chain lengths were observed with TGA and DSC studies respectively. Figure 6 reveals the thermal stability of the ionic liquids. In TGA-MS studies, only one step corresponding to the vaporization of the ionic liquids were obtained. The simultaneous mass analysis displayed no carbon monoxide formation and a negligible emission of carbon dioxide that can be attributed to the impurity present in the nitrogen purge gas. A chain length of 10-12 carbon atoms had the perfect balance between solubility, critical micelle concentration (CMC) and thermal stability. Surface tension (s.t.) studies were done to determine CMCs of the surfactants. The solubilities of the surfactants having tail lengths 18 and higher decreased. The synergism between positively and negatively charged surfactants were studied using the surface activity of their mixture as a probe (Figure 7). In order to determine the surface activity of a mixed surfactant system, water was first titrated with one surfactant solution until the surface tension (s.t.) reaches a constant value, after that a second surfactant solution was added to the previous solution and the change in surface tension was monitored. The surface tension of water at 22 ºC is about 72 mN/m. Upon addition of choline dodecylbenzenesulfonate (ChDBS) to water, s.t. decreased to 34.96 mN/m. Thereafter, the solution was titrated with a solution of C_1C_{10}ImCl. The surface tension of this ternary mixture reduced further to 25.2 mN/m, after which a white

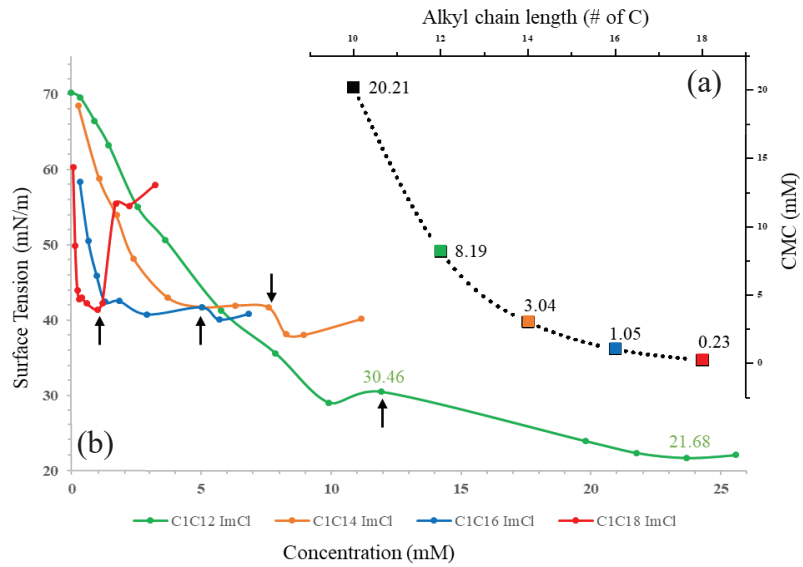

Figure 7. *(a) CMC decreases with increasing tail length. (b) Decrease in S.T. of water with increase in IL concentration. The black arrow indicates the start of addition of SDS.*

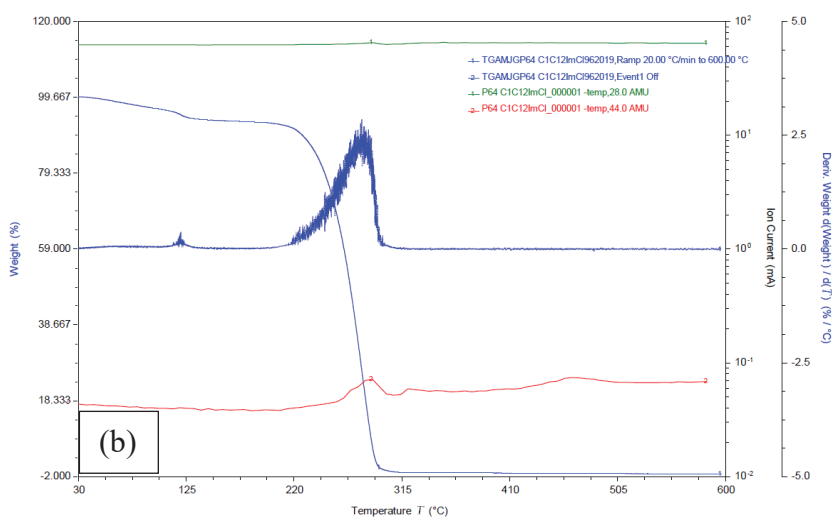

Figure 6. *TGA-MS study of C_1C_{12}ImCl.*

precipitate started forming. The white precipitate was formed as a result of salt formation between the oppositely charged organic heads. Therefore, it is evident that until the threshold of salt-formation is reached, electronic complementarity of the surfactants boosts the surface activity of the overall mixture. The synergism arises because oppositely charged head groups help alleviate the repulsion between the similarly charged heads of the SAILs/surfactants and thereby resulting in an increase in the number of surfactant molecules at the air-water interface. In a similar experiment, we first added $C_1C_{10}ImCl$ to water to achieve the lowest surface tension of 29.44 mN/m and followed up with addition of sodium dodecylsulfate (SDS) solution to achieve an overall reduced s.t. of 24.29 mN/m. Hence, the order of addition of two oppositely charged surfactants does not have much effect on the overall outcome. $C_1C_{12}ImBr$ reduced the s.t. of water to 34.42 mN/m and addition of SDS to the same solution further reduced the s.t. to 21.68 mN/m. Although, s.t. values of less than 25 mN/m were achieved with Im-SAILs with C_{10} and C_{12} tails in presence of SDS, the higher analogs such as C_{14}, C_{16} and C_{18} Im-SAILs were not able to reduce the surface tension below 30 mN/m. The interfacial tension between cyclohexane and a solution of 80:20 mol% $C_1C_{12}Im^+$-SAIL and SDS was 0-0.5 mN/m (Figure 8). Therefore, the surfactant mixture solution has a positive spreading coefficient over cyclohexane whose surface tension at 22 ºC is 25 mN/m. The equation for spreading coefficient (S) is, $S = \gamma^{FA} - (\gamma^{WA} + \gamma^{WF})$; where γ^{FA}- surface tension of hydrocarbon fuel, γ^{WA}- surface tension of surfactant solution, γ^{WF} - Interfacial tension between surfactant solution and fuel. The spreading coefficient of this particular mixture of surfactants over cyclohexane is 3.32 mN/m which meets the criteria enforced by MIL-PRF-24385F (SH). Addition of SDS had even severe synergistic effect on the surface tension of pyridinium-based SAILs.

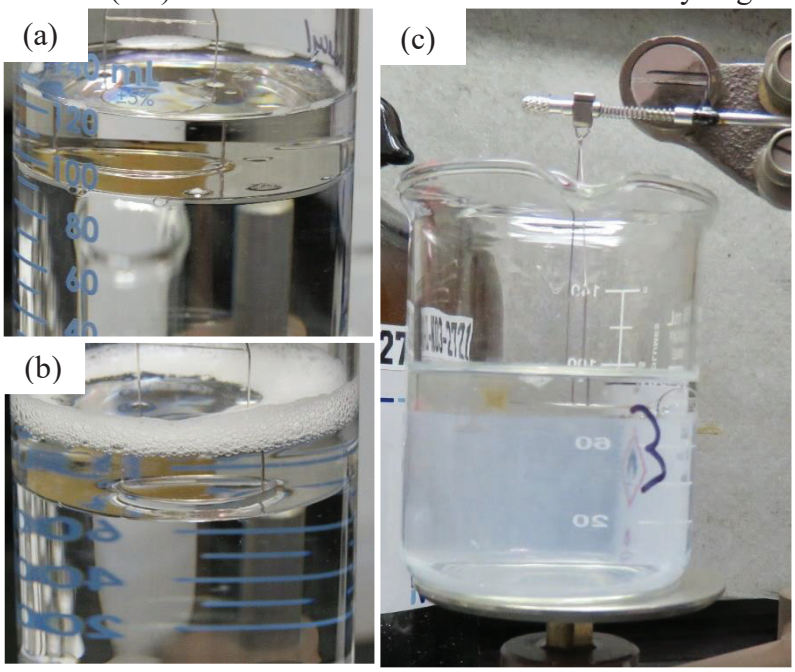

Figure 8. *Interfacial tension by DuNouy Ring method between cyclohexane and (a) $C_1C_{12}ImCl$ solution is 1 mN/m, (b) SDS solution is 4-5 mN/m, (c) 80:20 mol% mixture of $C_1C_{12}ImCl$ and SDS is 0-0.5 mN/m. Pictures were taken right before the meniscus break.*

The lowest surface tension achieved by addition of a solution of C_{12}-pydinium SAIL to water was about 38 mN/m (Figure 9). The surface tension was further reduced to a value of 23.24 mN/m upon addition of SDS. The final mixture had 85:15 mol% of pyridinium-SAIL and SDS. The solution turned murky and white flakes started to appear. Although, the precipitation did not have any effect on surface tension which remained constant at the lowest value, it may have negative effect on the foam stability and shelf-life of the formulation. To circumvent the event of precipitation, a sulfo-betaine zwitterionic liquid (ZIL), *N*-Dodecyl-*N, N*-dimethyl-3-ammonio-1-propanesulfonate was used. Interestingly, negligible turbidity was observed and the solution containing SAILS/surfactants with oppositely charged head groups, e.g., C_1C_{12}ImCl and SDS, remained clear.

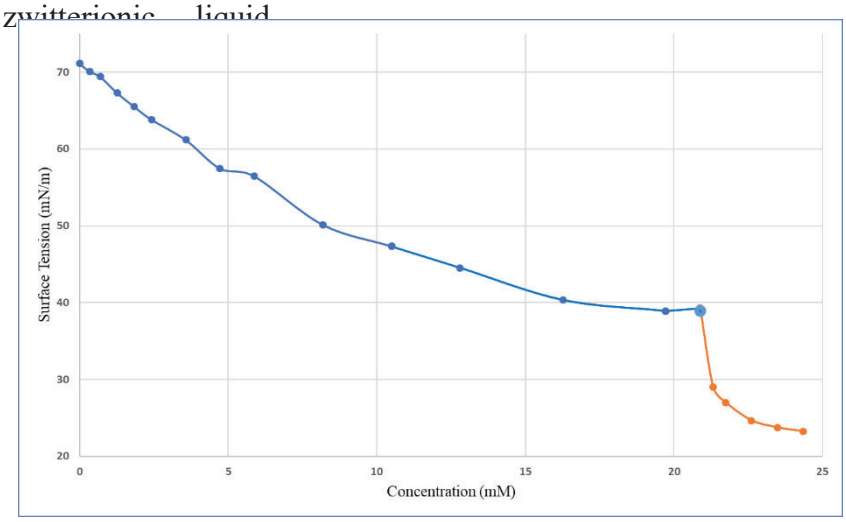

Figure 9 *Effect of C_{12}-Py$^+$- salts alone (blue line) and with SDS (orange line) on the surface tension of water.*

In order to nanoencapsulate SAILs, the IL was stirred in water in presence of a co-surfactant. The cosurfactant was chosen such that they can bind metal ions such as Mg^{2+}, Ca^{2+}, etc. One such cosurfactant used was Brij S-20, which has polyethyleneglycol (PEG) moieties to form chelate with the metal ions. The co-micellization of the binary surfactant mixture furnished the required template for the carbonate shell to form. Figure 10 displays the TEM image of the core-shell structure of the NEILs. The presence of IL at the core was confirmed by ESI-MS. Before recording ESI-MS, the NEILs were washed thoroughly with distilled water until no white precipitate was formed with $AgNO_3$ solution. The effort to modify the surface of the NEILs to introduce appropriate degree of hydrophobicity is underway.

Figure 10. *TEM micrographs of NEIL-1*

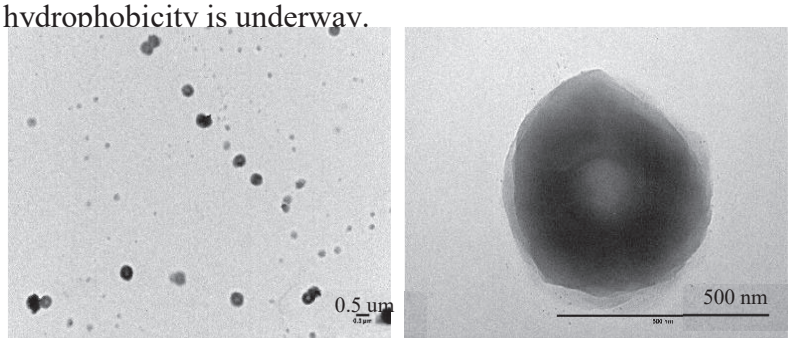

Foam stability tests indicate that addition of 10-20 mol% SDS has definitive stabilizing effect on the foam generated by $C_1C_{12}ImCl$ (Figure 11). While the 25% foam drainage time of 2 wt% $C_1C_{12}ImCl$ solution was 3.6 min under the experimental conditions, it increased to 3.9 min in presence of 0.1 wt% SDS. The 25% foam drainage time of only $C_{12}PC$ was a little above 2 mins under the experimental conditions. The 25% foam drainage time for 1 wt% KPFOS solution was 1.0 min which is worse than the surfactants and mixtures that we have used (Figure 11). We also found that foam generated by SAILs/surfactants displayed improved stability in the presence of nanoparticles. The foams containing nanoparticles were stable for several hours. Figure 12 shows the microscopic images of $CaCO_3$ nanoparticles. Both solution method and ball-milling produced nanoparticles with average diameter below 100 nm. The already enhanced stability of

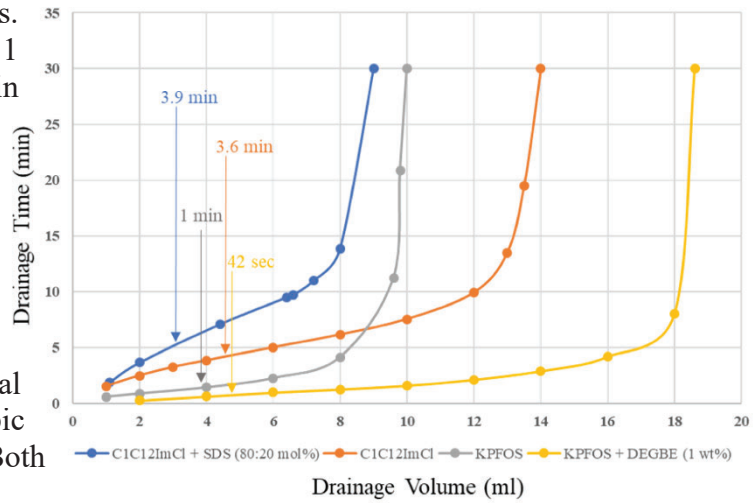

Figure 12. *Foam drainage study of 1-dodedcyl-3-methyl imidazolium chloride and mixture of 1-dodedcyl-3-methyl imidazolium chloride and SDS.*

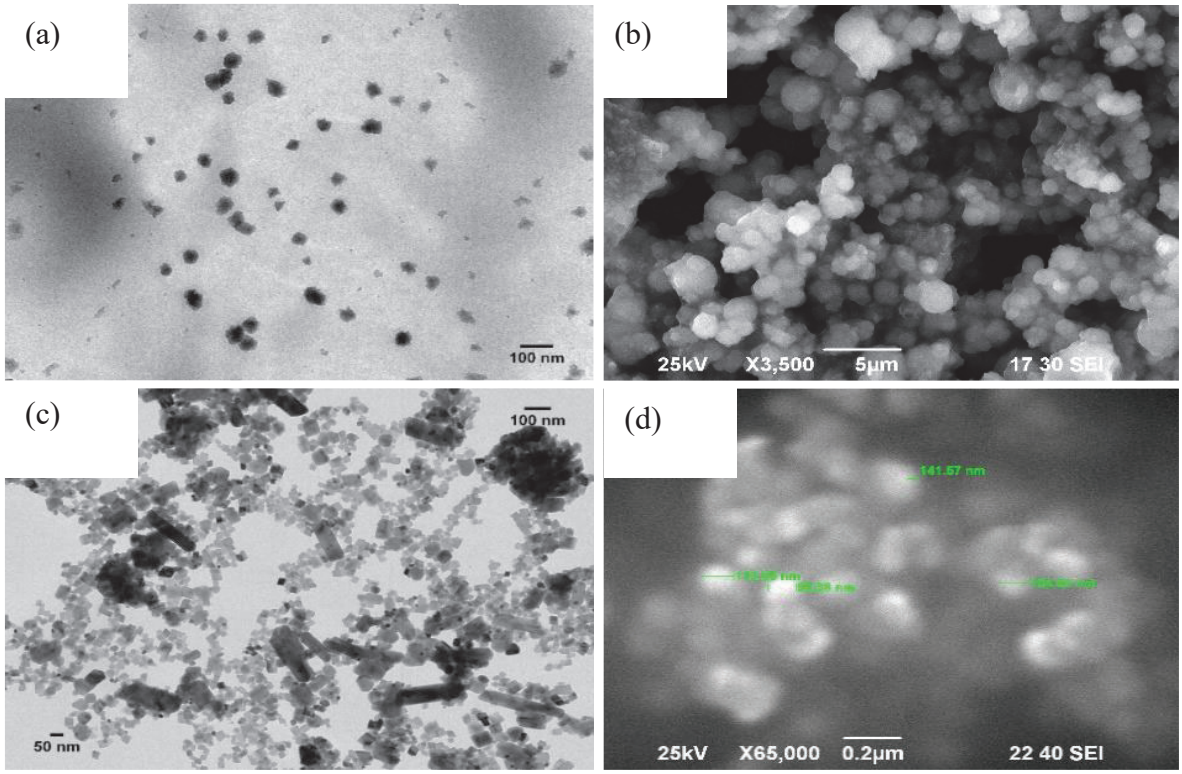

Figure 11. *(a) and (b) are TEM and SEM micrographs of $CaCO_3$ NPs synthesized by solution method; (c) and (d) are TEM and SEM micrographs of $CaCO_3$ NPs produced by ball milling.*

the foam generated by a mixture of SDS and SAIL was further improved by NEIL-1. During the course of these experiments, precipitation of salts was observed when two oppositely charged surfactants were mixed. The problem was solved by using a zwitterionic surfactant. In presence of the zwitterionic surfactant, the mixture remained visually clear to a wide ratio of the oppositely charged SAILs/surfactants while a ST in the 21-23 mM/m was achieved.

Fire testing

A preliminary fire test with 1 wt% solutions of 1-dodecyl-pyridinium chloride, and their mixture with SDS in different proportions of has shown excellent fire-fighting potential. Photography and videography were done to document the experiments (Figure 13 and Figure 14).

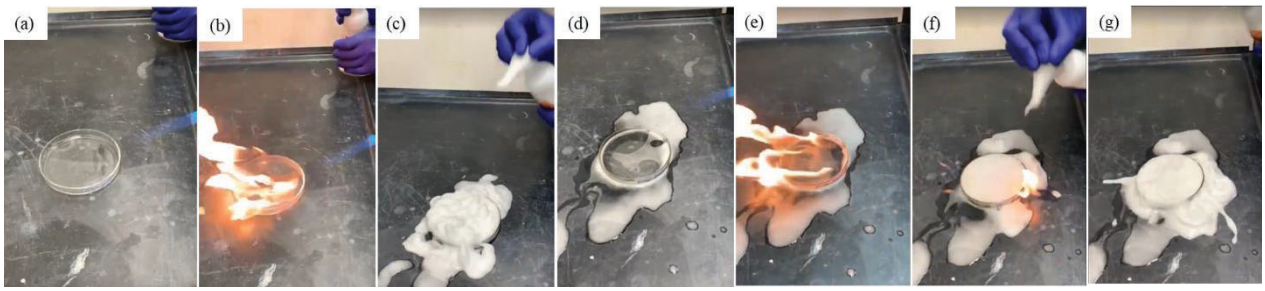

Figure 13. *Cyclohexane was taken in a petri dish (a) and flamed by a torch to generate fire (b). The fluorine-free foam formulation was then dispensed over the fire by a hand soap dispenser to completely extinguish it (c). The foam blanket was torched continuously (d). Although the foam started wane away, the probable existence of an aqueous layer on top of cyclohexane kept the fuel underneath from catching fire (d) for some time, after which the fuel got reignited (e). The foam was again dispensed like before (f) and the fire got extinguished (g).*

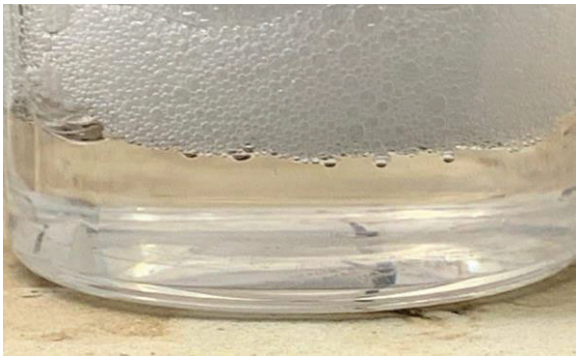

Figure 14. *Foam blanket floating over cyclohexane.*

Computational modeling of interfacial properties of aqueous solutions of surfactants

Model validation

To validate our model, we computed the surface tension of water, cyclohexane, and interfacial tensions at the water/cyclohexane interface. Our value for the surface tension computed using Eq. 2 for the TIP4P/2005 water at 298 K is around 66 mN/m, which is about 6 mN/m lower than the experimental value. This result is consistent with the value reported in the literature for TIP4P/2005 without tail correction[45]. The computed surface tension of cyclohexane is 16 mN/m, which is about 8 mN/m lower than the experimental value. Our computed value of interfacial tension of cyclohexane and water is 48 mN/m vs. the experimental value of 50.2 mN/m[54]. We note that the experimental spreading coefficient for cyclohexane over pure water is -98 mN/m while

our computed value is around -98 to -95 mN/m. Surface tensions of a set of pure organic liquids were evaluated using molecular dynamics with the GAFF force field[42]. This forcefield is known to systematically underestimates experimental surface tensions.

Interfacial properties of sodium perfluorooctanoate aqueous solutions.

Interfacial properties of surfactant solutions depend on the surface coverage of the surfactant adsorbed at the interface. Sodium perfluorooctanoate is a well-studied perfluorinated surfactant, which is used in current AFFF formulations.[55] The surface tension of its aqueous solutions as a function of the coverage can be derived from experimental measurements of the surface tension as a function of the bulk concentration and adsorption isotherms derived from neutron reflectometry[55]. Figure 15 compares experimental results[55] and our model predictions. Our model systematically underestimates the experimental surface tension as a function of the surface coverage. The root mean squared error for coverages below 3.7 μmol/m^2 is 8 mN/m. A significant contribution to this error is systematic underestimation. The predicted minimum surface tension of 15 mN/m also underestimates the experimental value of 22.6 mN/m[55]. However, the predicted and experimental limiting coverages and the coverage when the adsorption layer becomes to buckle in the direction normal to the interface agree very well (both quantities are around 4 μmol/m^2). It is likely that in the absence of finite size effects due to periodic constraints, the layer would become unstable at higher coverage.

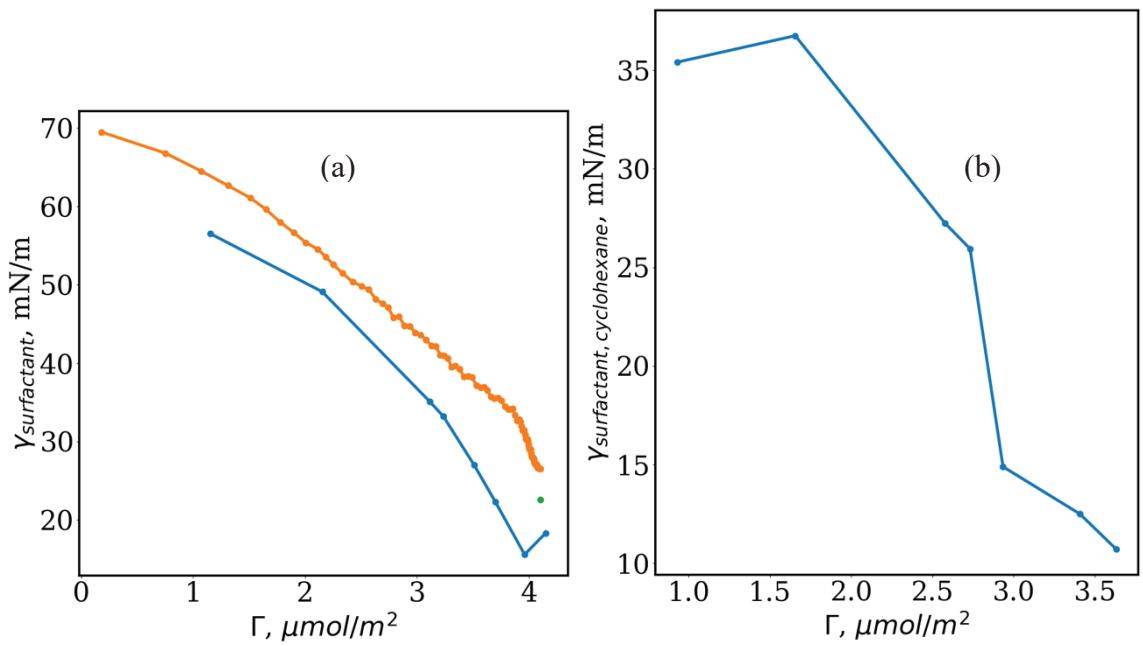

Figure 15. *(a) A comparison between experimental (orange) and the theoretical (blue) surface tension vs. the surface coverage for sodium perfluoreoctanate[55]. The experimental adsorption isotherm derived from the neutron reflection experiments[55]. The green dot points to the experimental minimum of the surface tension. (b) The computed interfacial tension vs. surface coverage.*

We also investigated the structure and dynamics of sodium perfluorooctanoate adsorption layers for a range of surface coverages (see Figure 16(a-h)). The hydrophobic tails of PFOA anions point away from the aqueous solution during our simulations. Islands of PFOA anions are dynamically

forming and decaying independently at lower coverages (<3 μmol/m^2), the dynamics of the layer gradually transitions to a collective regime at higher coverages. A monolayer (1 ML) of PFOA anions, which is well organized in the direction normal to the interface, forms at the limiting coverage of around 4.0 μmol/m^2. The adsorption layer at higher coverages buckles, and some of PFOA anions migrate into the bulk of the aqueous solution. The surfactant anion would likely prefer to form micelles rather than adsorb beyond this loading. The adsorption layer features a short-range order as the radial distribution function of the hydrophilic carboxylate groups indicates (see Figure 17). Sodium cations spend most of the time near the carboxylate anions, although there is a considerable chance of finding sodium cations traveling far from the carboxylate groups in the solution (see Figure 18). In particular, we observed that cation-anion pairs dynamically associate, likely because of the attractive dipole-dipole interaction.

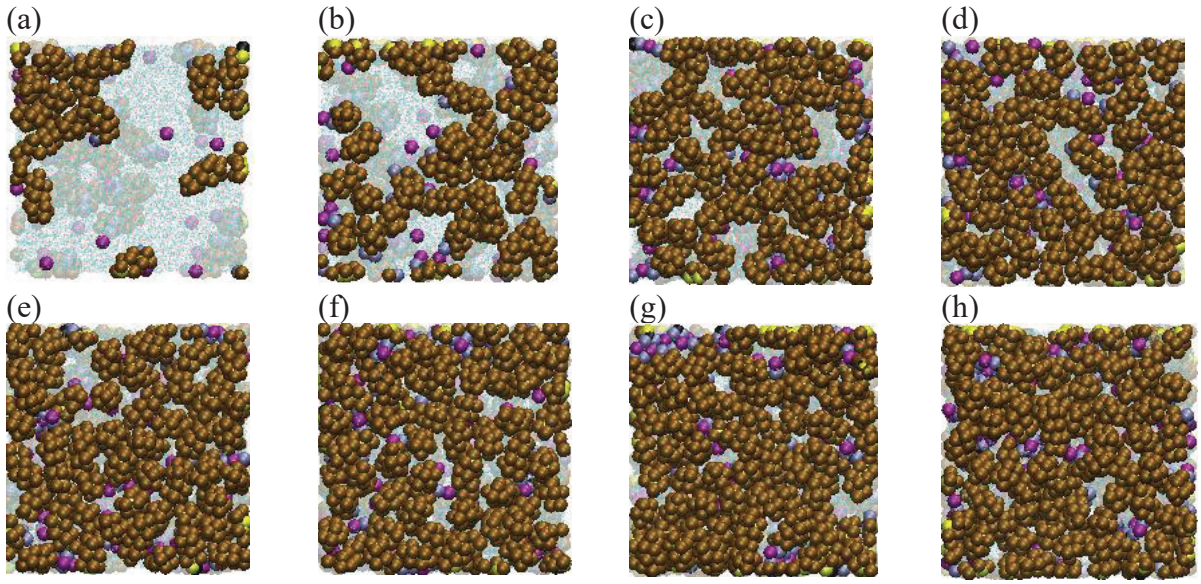

Figure 16. *Adsorption layer structure vs. the surface coverage for sodium perfluorooctanoate at different surface coverages. (a)Γ=1.15 μmol/m^2; (b) Γ=2.15 μmol/m^2; (c) Γ=3.11 μmol/m^2; (d)Γ=3.23 μmol/m^2; (e)Γ=3.51 μmol/m^2; (f)Γ=3.70 μmol/m^2; (g)Γ=3.96 μmol/m^2; (h) Γ=4.15 μmol/m^2. Hydrophobic tails and sodium cations are shown in ochre and purple, respectively. Water molecules are shown as blue dots for the sake of clarity.*

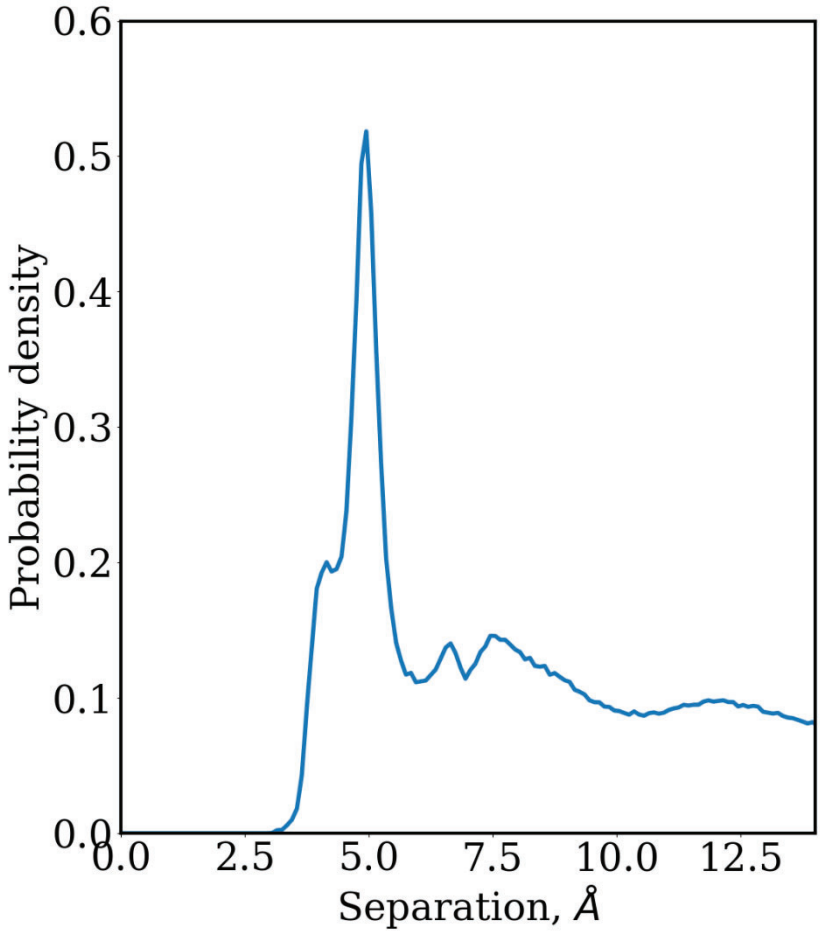

Figure 17. *The radial distribution function for carboxylate-carboxylate separation in a layer of PFOA anions in the adsorption layer around the saturation coverage of 4 μmol/m^2.*

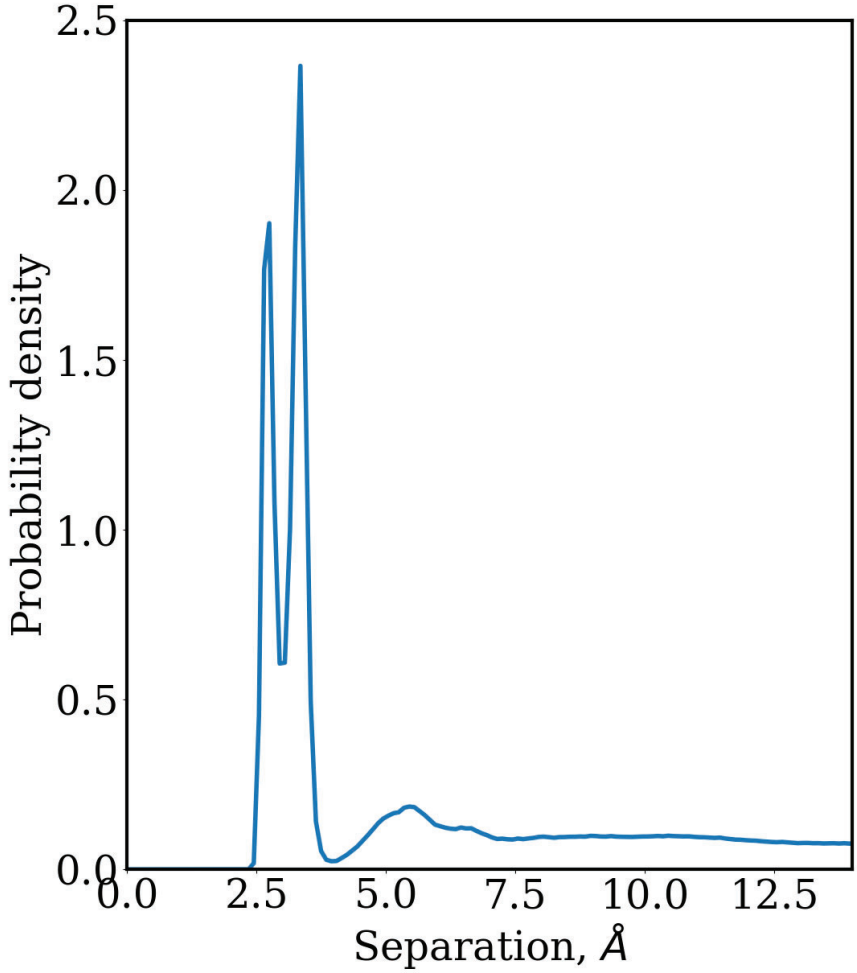

Figure 18. *The radial distribution function for carboxylate-sodium separation in a layer of PFOA anions in the adsorption layer around the saturation coverage of 4 μmol/m^2.*

Interfacial properties of 3-alkyl-1-methyl imidazolium aqueous solutions.

We examined in detail adsorption layer structure, dynamics as well as surface and interfacial tensions of 3-alkyl-1-methyl imidazolium chlorides with the alkyl chain lengths of 6, 8, 10, 12, 14, and 16 atoms. All 3-alkyl-1-methyl imidazolium chlorides adsorb at the surface with imidazolium head groups solvated and alkyl tails pointing outside of the aqueous phase. As a radial distribution function for the separation between the hydrophilic head groups in Figure 20 indicates, the arrangement of the hydrophilic head groups of 3-alkyl-1-methyl imidazolium cations adsorbed at the vapor-aqueous solution interface does not exhibit noticeable short-range order of the kind that we observed in the case of sodium perfluorooctanoate. Chloride anions are mobile in the aqueous phase near the interface but prefer to stay near the cations (see Figure 21). As the length of the hydrophobic alkyl chain increases, the likelihood that the 3-alkyl-1-methyl imidazolium cation migrate into the bulk of the solution diminishes.

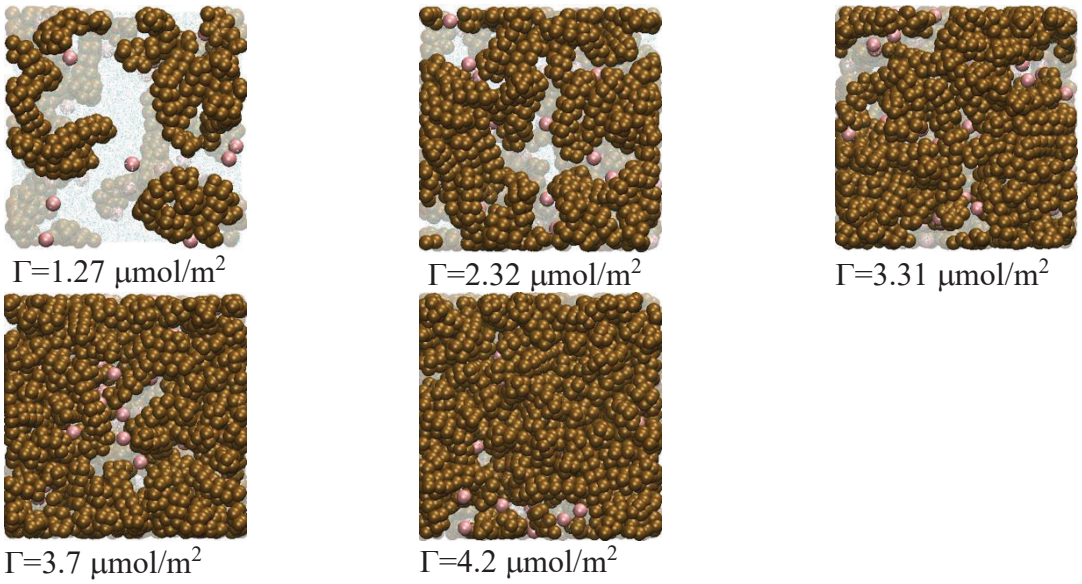

Figure 19. *3-dodecyl-1-methyl imidazolium chloride adsorption layer at various coverages. 3-Dodecyl-1-methyl imidazolium cations are shown in ochre. Chloride anions are shown in pink. The layer begins to buckle for coverages higher or around 3.7 μmol/m²*.

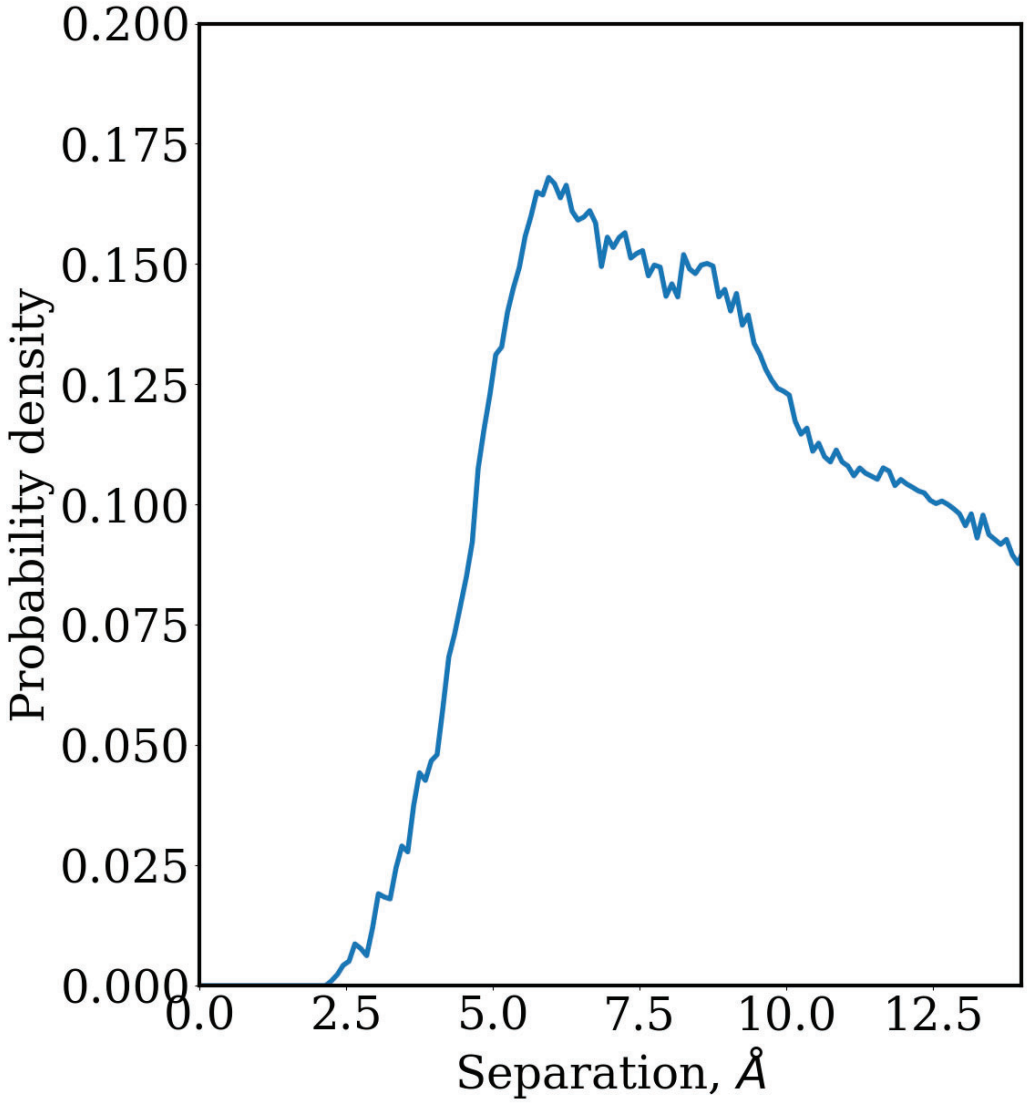

Figure 20. *The radial distribution function for separation between the head groups of 3-dodecyl-1-methyl imidazolium cations at 3.7 μmol/m^2 in an aqueous solution of 3-dodecyl-1-methyl imidazolium chloride.*

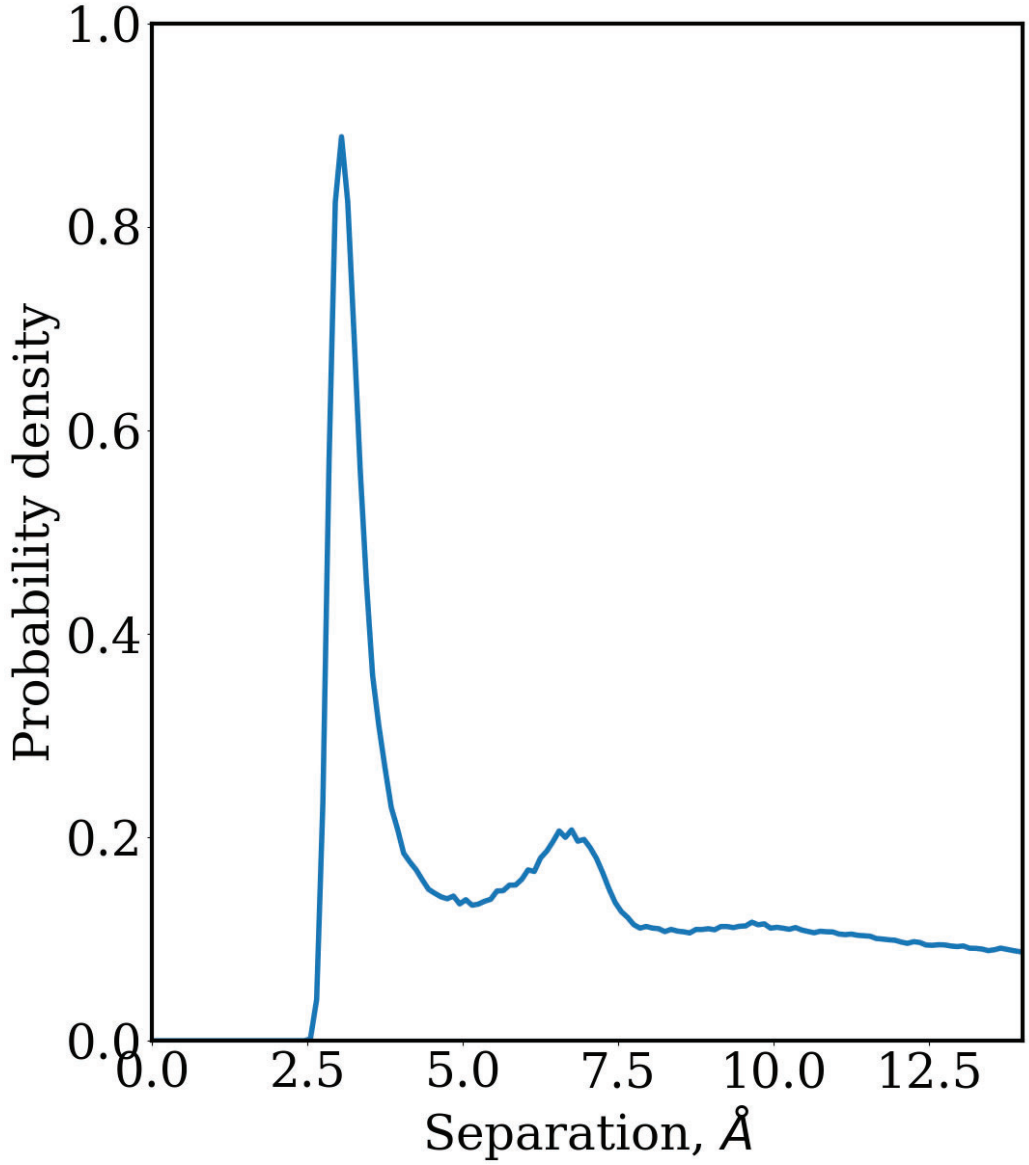

Figure 21. *The radial distribution function for separation between the head groups of 3-dodecyl-1-methyl imidazolium cations and chloride anions at 3.7 μmol/m² in an aqueous solution of 3-dodecyl-1-methyl imidazolium chloride.*

Figure 22 shows computed surface tension as a function of the surface coverage for 3-alkyl-1-methyl imidazolium chlorides with the alkyl chain lengths of 6, 8, 10, 12, 14, and 16 atoms. The surface tension first decreases as the length of the alkyl chain decreases and then increases as the number of carbon atoms in the chain further increases at surface coverages greater than 3 μmol/m². This trend also emerges in our experiments. 3-decyl-1-imidazolium chloride is the most effective in lowering the surface tension of water at coverages of 3-3.5 μmol/m², while 3-dodecyl-1-imidazolium chloride results in the lowest surface tension at coverages around 4 μmol/m². Since we do not know the exact value of the limiting coverages for 3-decyl-1-imidazolium and 3-dodecyl-1-imidazolium chlorides, we cautiously consider them in a tie for achieving the lowest surface tension among for 3-alkyl-1-methyl imidazolium chlorides. Furthermore, 3-decyl-1-

imidazolium and 3-dodecyl-1-imidazolium chlorides are comparable to sodium perfluorooctanoate in their ability to lower the surface tension for coverages greater than 3 μmol/m^2.

Computed interfacial tensions of an aqueous solution of 3-alkyl-1-methyl imidazolium chlorides over cyclohexane in Figure 23 decrease with the surface coverage. The trend is very similar for 3-alkyl-1-methyl imidazolium chlorides with 10 to 16 carbon atoms, and their interfacial tensions approach very low levels at coverages around 3 μmol/m^2. Furthermore, 3-decyl-1-imidazolium and 3-dodecyl-1-imidazolium chlorides are better than sodium perfluorooctanoate in their ability to lower the interfacial tension for coverages greater than 3 μmol/m^2. We observed negative values of interfacial tensions at coverages higher than 3 μmol/m^2. The latter likely indicates that the interface becomes metastable at those coverages, i.e., limiting coverage is no higher than 3 μmol/m^2 or the interface is unable to equilibrate at the time scale of our simulation.

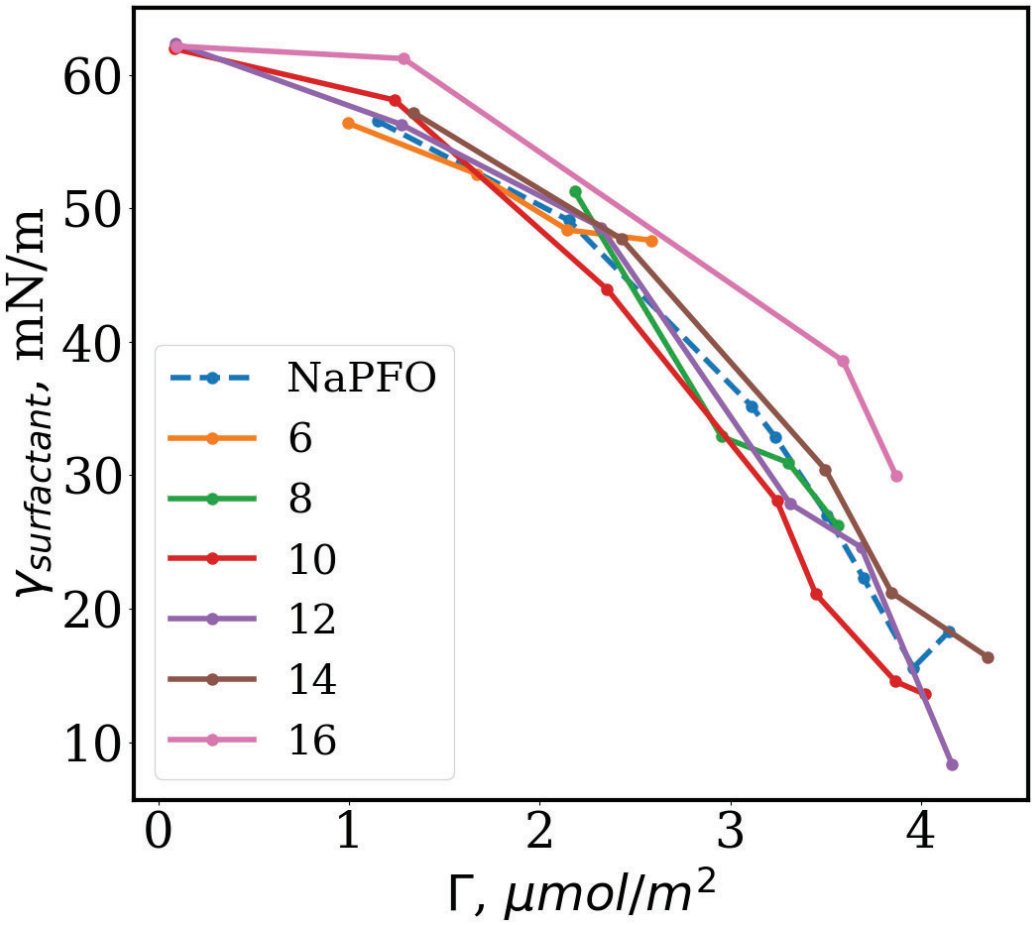

Figure 22. *Surface tension vs. the surface coverage for 3-alkyl-1-methyl imidazolium chlorides with 6, 8, 10, 12, 14, and 16 carbon atoms in the alkyl chain.*

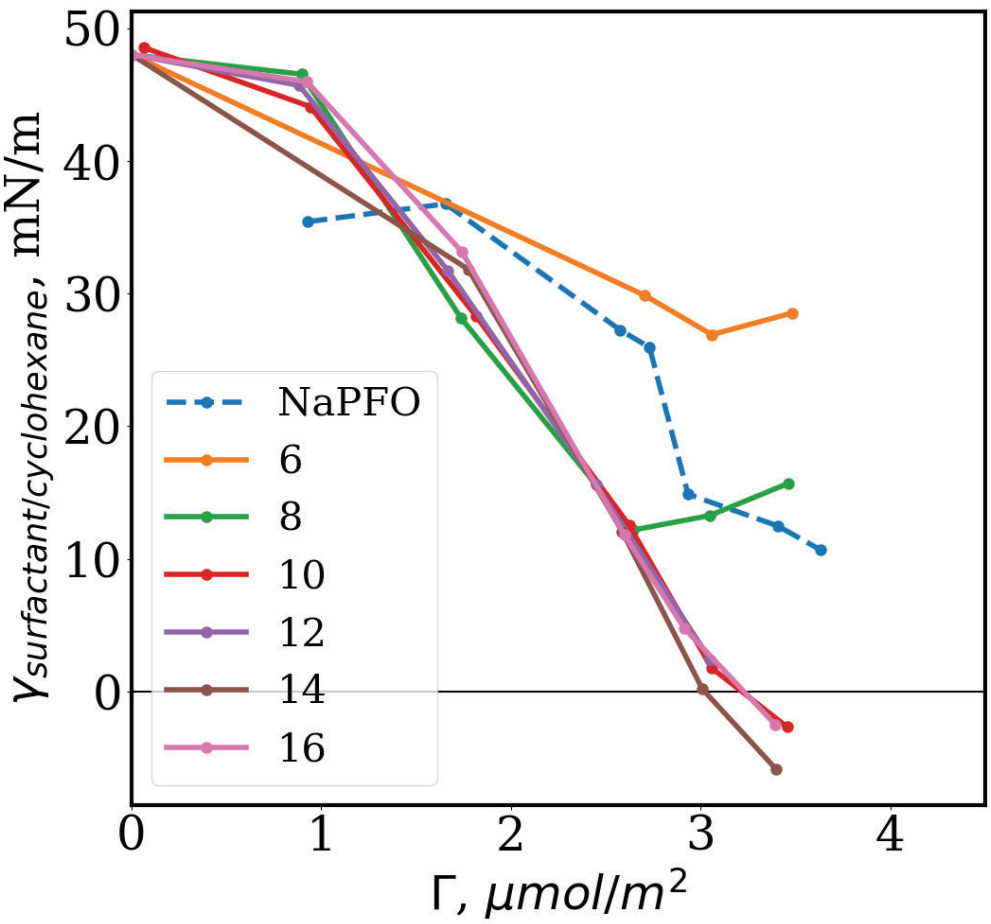

Figure 23. *The interfacial tension vs. coverage for 1-methyl-3-alkyl imidazolium chlorides.*

It follows from Figure 22 and Figure 23 that 3-decyl-1-imidazolium and 3-dodecyl-1-imidazolium chlorides have the potential to yield higher spreading coefficients than that of sodium perfluorooctanoate, a chemical that we aim to replace in the AFF applications.

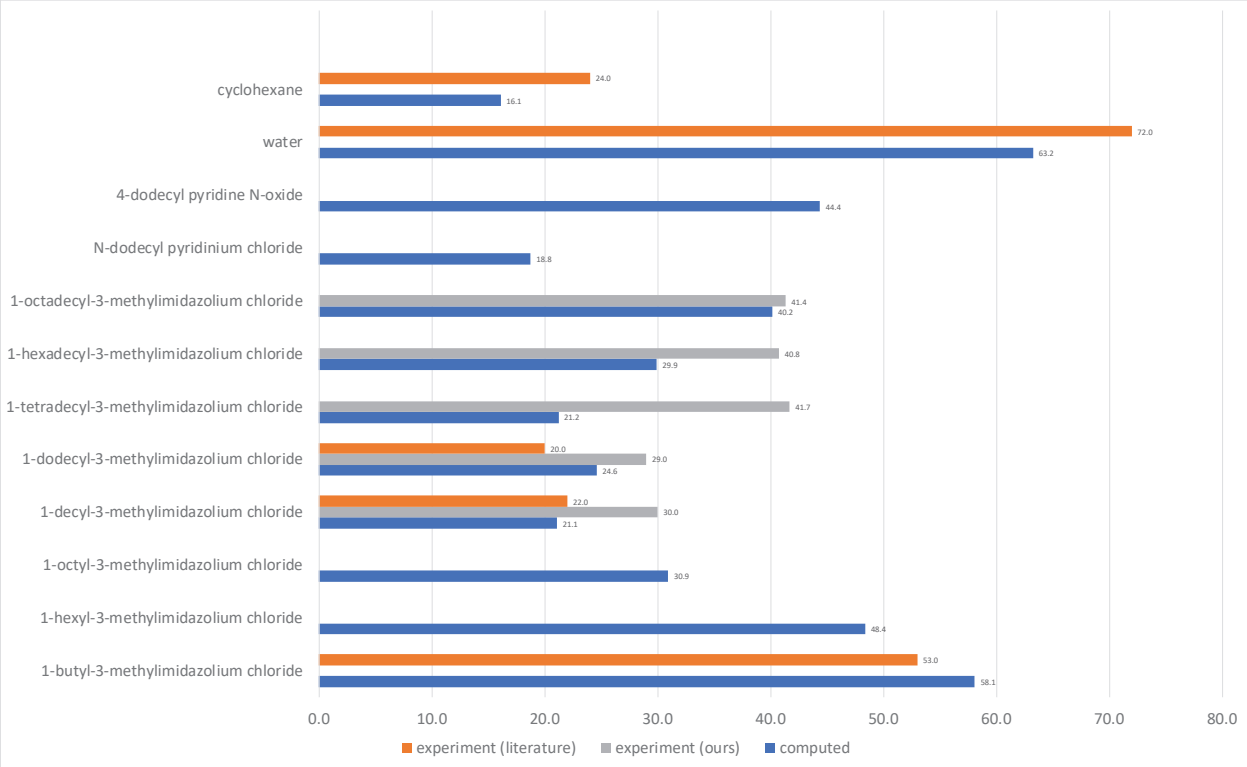

Figure 24. *Computed surface tensions for select surfactants at around 3.5 μmol/m²*

Screening over a broader set of surfactants

To screen the performance of other surfactants, we estimated their surface tension at coverages around 3.5 μmol/m^2 (see Figure 24). In addition to 3-alkyl-1-methyl imidazolium chlorides with 10-14 atoms, N-dodecyl pyridinium chloride is another ionic liquid surfactant, which is very effective in lowering the surface tension of water at this coverage.

Spreading coefficients over cyclohexane computed using Equation 4 are shown in Figure 26. We report two values of spreading coefficients. A lower value is computed using our computed value of the cyclohexane surface tension (16 mN/m). The other value is 8 mN/m higher. It relies on the experimental surface tension of cyclohexane. 3-alkyl-1-methylimidazolium chlorides with 10-14 carbon atoms show the highest spreading coefficients. Another ionic liquid, N-dodecyl pyridinium chloride, show the performance comparable to that of 3-alkyl-1-methylimidazolium chlorides with 10-14 carbon atoms.

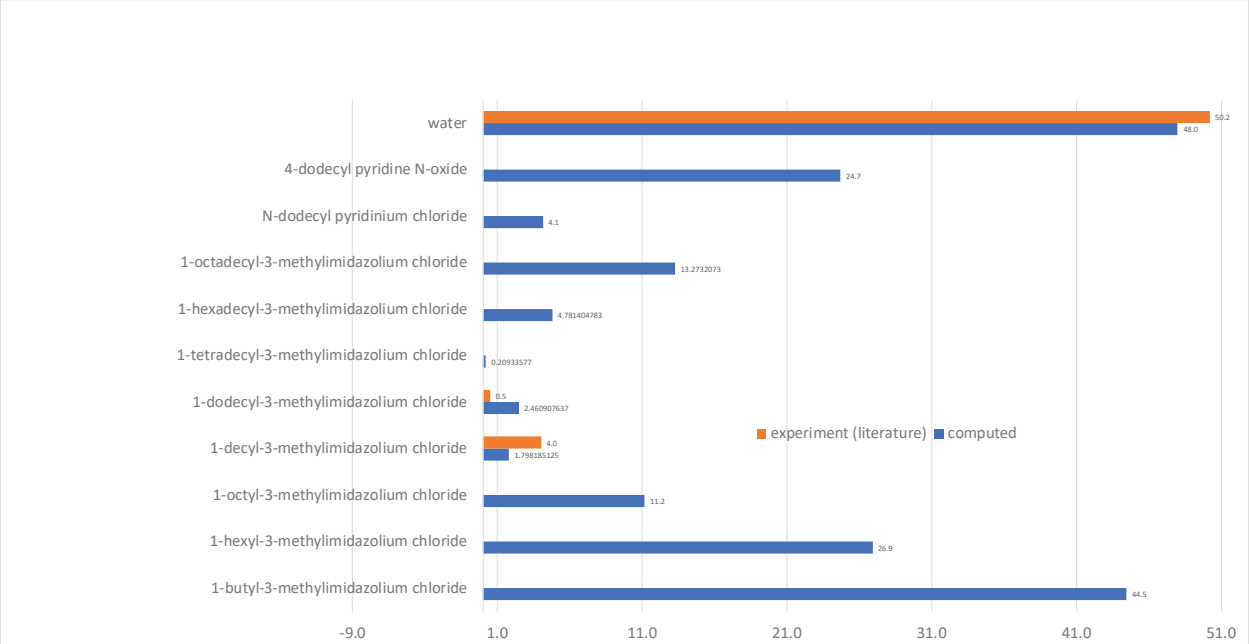

Figure 25. *Computed interfacial tensions for select surfactants.*

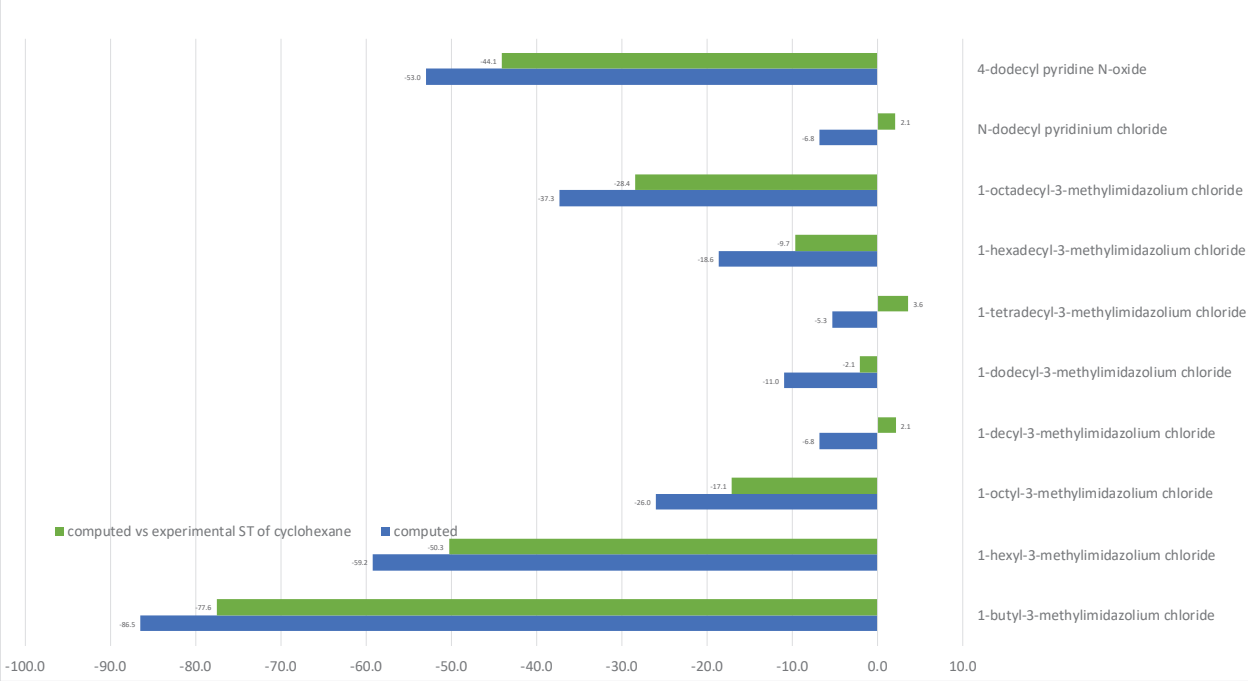

Figure 26. *Estimated spreading coefficients for select surfactants.*

Cohesive enthalpies and densities.

Our model successfully reproduces experimental densities of 3-alkyl-1-methyl imidazolium chlorides with an error less than 10%. To estimate the volatility of 3-alkyl-1-methyl imidazolium chlorides, we computed their standard cohesive enthalpies using Eq. 4. The results are shown in Table 2. As a reference we computed the standard enthalpy of vaporization of water. TIP4P/2005 water reproduces the exact enthalpy of vaporization of water. Cohesive enthalpies of 3-alkyl-1-methyl imidazolium chlorides increase with the number of carbon atoms in agreement with the observable trends in the melting temprature. The enthalpies are a factor of 4.7-5.6 higher than those of water at standard conditions. As a consequence, the vapor pressure of these ionic liquids is negligible at standard conditions.

Table 2. *Standard cohesive enthalpies and densities of select ionic liquids.*

Substance	Computed $\Delta H^{\circ}_{cohesive}$, in kcal/mol	Experimental $\Delta H^{\circ}_{cohesive}$, in kcal/mol	Computed density, kg/m^3	Experimental density, kg/m^3
1-butyl-3-methyl imidazolium chloride	47.0	-	994	1086
1-hexyl-3-methyl imidazolium chloride	48.3	-	966	1030
1-octyl-3-methyl imidazolium chloride	49.8	-	944	1010
1-octyl-3-methyl imidazolium chloride	52.1	-	927	990
1-dodecyl-3-methyl imidazolium chloride	52.7	-	916	-
1-tetradecyl-3-methyl imidazolium chloride	56.4	-	909	-
1-hexadecyl-3-methyl imidazolium chloride	58.7	-	901	-
1-octadecyl-3-methylimidazolium chloride	59.9	-	882	-
Water	10.5	10.5	991	

Adsorption of surfactants at magnesite surfaces.

We need surfactants that bind to magnesium carbonate nanoparticles and form NEIL. For this to happen, our surfactants need to bind strongly to the outer shell of nanoparticles or bind weakly to the inner shell. Here, we used density functional theory to rank with respect to the binding energy various surfactants' head groups to the surface of magnesite.

Molecular modeling has been used to study interactions of organic molecules at calcite surfaces since as early as 2004 by Duffy and Harding[56], and de Leeuw and Cooper[57], primarily examining how interactions of the mineral with organic molecules effect the growth of the crystal. Freeman et al. studied interactions of organic molecules at the calcite and magnesite surfaces in aqueous solution in 2009[58] and showed that in general the binding of formic acid is stronger than that of methylamine on both minerals in aqueous solution. Also, they showed that the geometry of the mineral surface plays a major role in the efficacy of binding for these molecules, and that there was very little or exclusively repulsive binding between the molecules and various less common magnesite surfaces. Ataman et al.[59] computed the binding energy of various sulfur, nitrogen and oxygen containing organic molecules (without water) using periodic DFT and DFT-D2.

Results from experimental work of Thomas et al.[60]showed that the chemicals with some of the highest surface coverage on calcite, dolomite and magnesite were alkyl-chain amines (*n*-decylamine, hexadecylamine and hexadecylamine respectively) though this coverage was easily reversible using appropriate solvent. The overall strength of adsorption determined from their study was carboxylated polymers and fatty acids > dicarboxylates and long-chain sulfonates > alcohols, sulfonates and amines. Amino acids and short-chain carboxylates were shown to have little or no adsorptive behavior. The main takeaway from these results seems to be that amines exhibit some of the strongest binding to the mineral surfaces – but only in cases where there is no competition with water or other solvent that provides high solubility of the amines. Since the most common solvent for fire-fighting applications is water, we endeavored to examine other chemical structures (such as those that exist in long alkyl chain ionic liquids) that may provide strong binding to the mineral in an aqueous environment such that robust nanoparticles can be formed that have a foam-forming effect for fire suppression.

Description of binding configurations at mineral surfaces

Table 3 lists binding energies for model systems, which are also shown in Figure 28-Figure 36. The strongest binding molecules in general are those containing carboxyl or anionic oxygen atoms. It is important to note that the binding energies reported in Table 2 (and some of those reported in Table 1) represent one geometric configuration of the mineral+water+molecule system and is therefore one of many measurable binding energies.

The numbers reported in Table 2 are minima resulting from periodic DFT calculations accounting for dissolution in water, so it can be expected that the results are a reasonable indicator of the solvated binding strength of the molecules in water, but it is possible that some of these values represent a local minimum of the energy surface and therefore are not representative of the molecule's strongest binding in a fully comparative way. Since these are 0 K optimizations, sampling of realistic thermal environments was not undertaken in this study. The water molecules

coordinate to a frozen hydrogen-bonded network in every optimization, leaving little room for exploration of different geometries resulting from variation in the many degrees of freedom of the system. An ideal metric of the interaction energy of the molecules in aqueous solution with the surface would arise out of some metadynamics calculations after sampling many configurations over a large timescale. Based on our calculations summarized in Figure 27, 3-alkyl-1-methyl imidazolium and 1-alkyl-pyridinium ionic liquids should bind to magnesite relatively weakly, and therefore are ideal for inclusion within magnesite nanocapsules. Upon rapture of these capsules, the ioninc liquids would readily be released which will heal defects in the firefighting film. On the other hand, stronger binding surfactants such as alkyl hydroxamic acid, alkyl sulfates, and alkyl sulfonates can be used to ensure a stable suspension of nanoparticles in the surfactant solution.

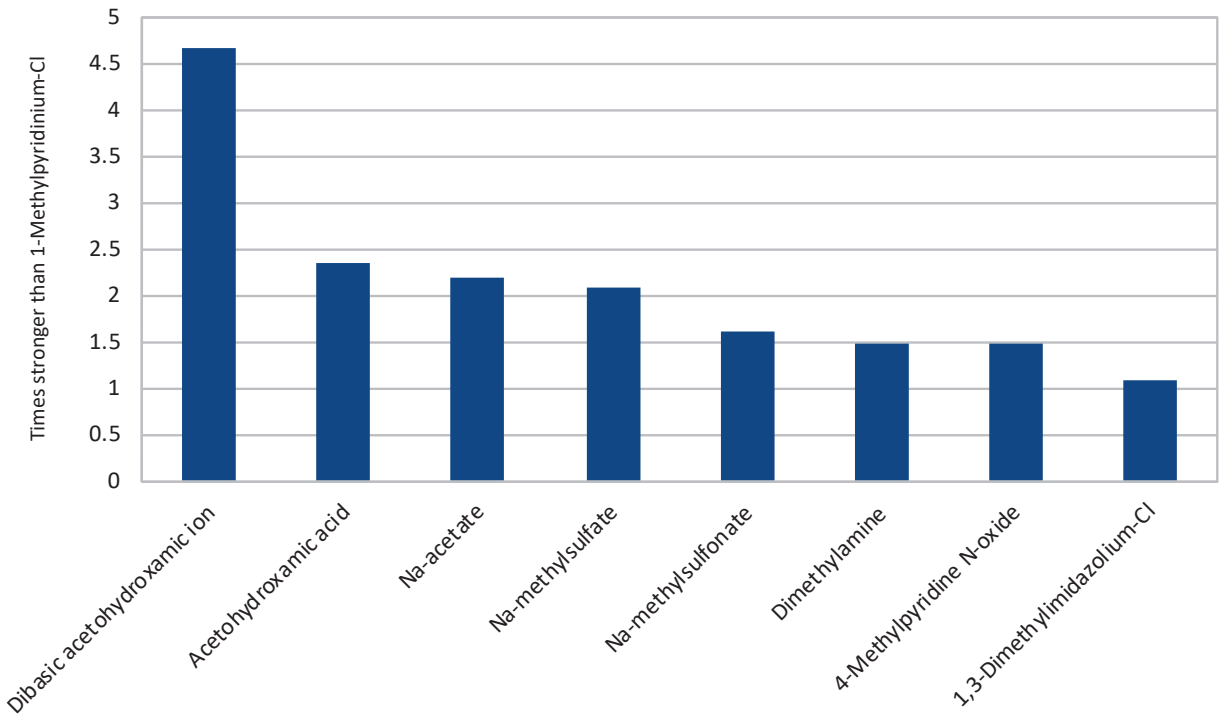

***Figure 27**. Relative binding energies of various head groups at the (10.4) surface of magnesite.*

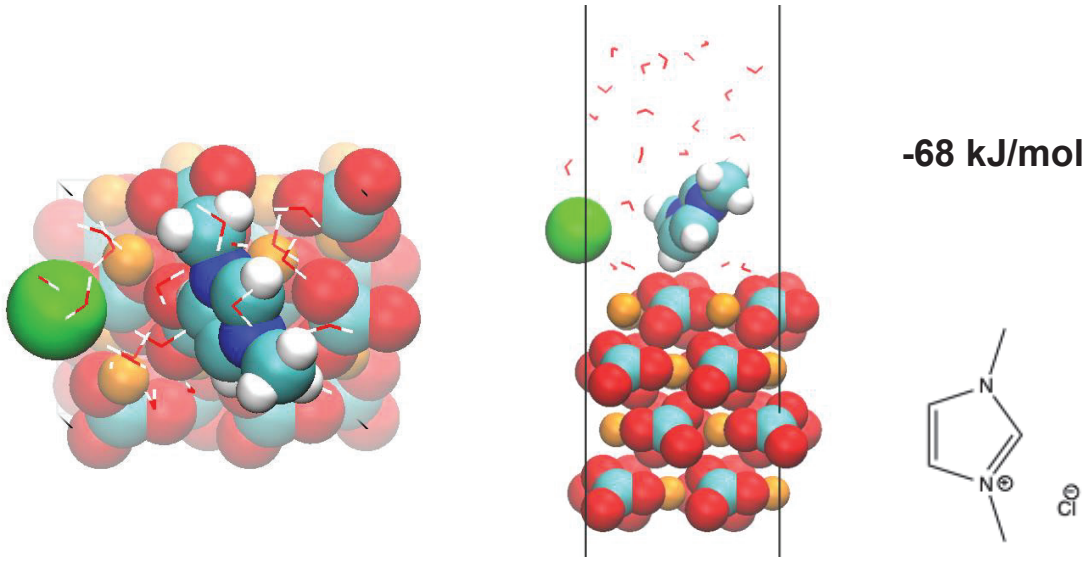

Figure 28. *Binding geometries for 1,3-Dimethylimidazolium chloride. The imidazolium planar ring structure aligns itself almost orthogonally (90°) to the magnesite (10.4) surface. In both cases the molecule is able to fit between the water molecules on the first layer, which are coordinated to the metal ions via M—O_{H2O} interactions. The chloride ion is solvated and further displaced from the surface than the cation. The closest interactions of imidazolium and the surface are $H_{imidazolium}$—$O_{mineral}$.*

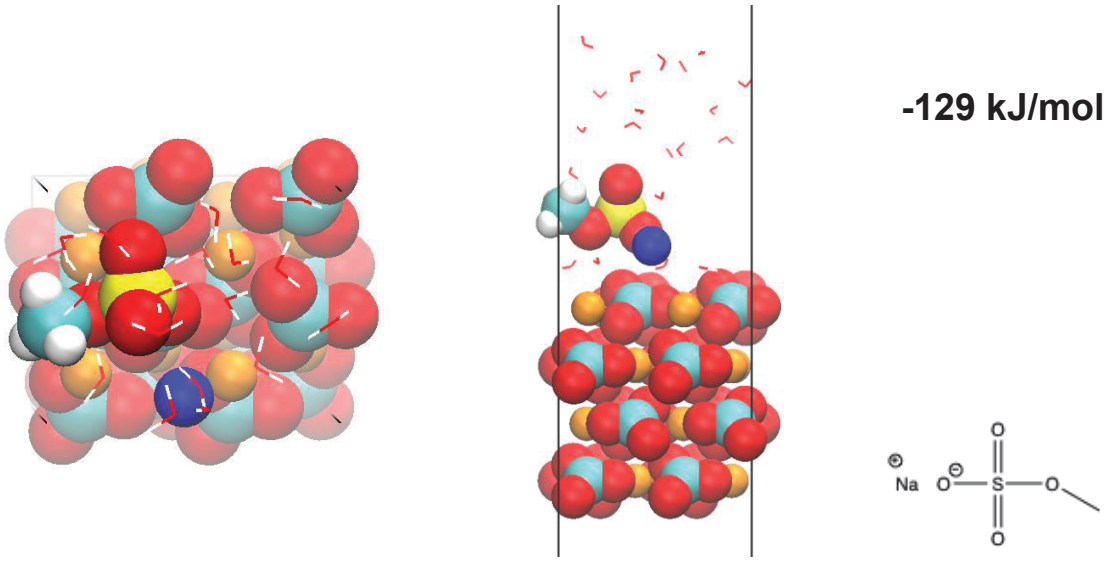

Figure 29. *Binding geometries for sodium methylsulfate. The sulfate group is closest to the (10.4) surface of the magnesite, with concurrent O—$Mg_{magnesite}$ interactions. The sodium ion coordinates to the carbonate oxygens on the surface, while at once being solvated by interactions with O_{H2O}.*

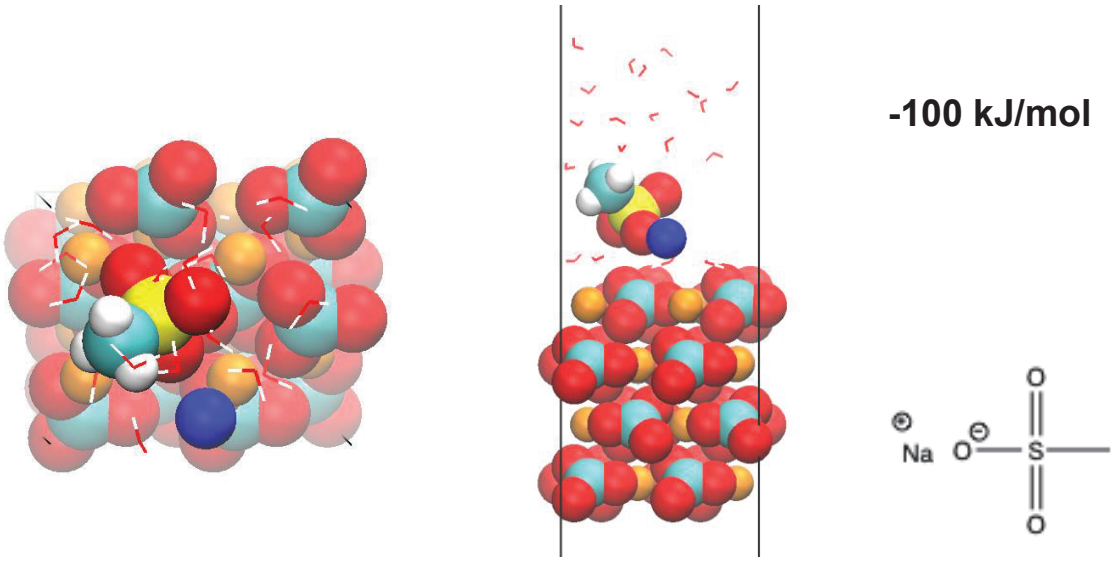

Figure 30. *Binding geometries for sodium methylsulfonate. The methylsulfonate anion orients itself with the sulfonate group attracted to the surface at a ~45° of the S—C bond to the plane of the surface, again with concurrent* $O_{sulfonate}$*—metal interactions. The sodium ion orients itself to the carbonate oxygens on the surface, while simultaneously being hydrated by water molecules and interacting with the sulfonate group as well.*

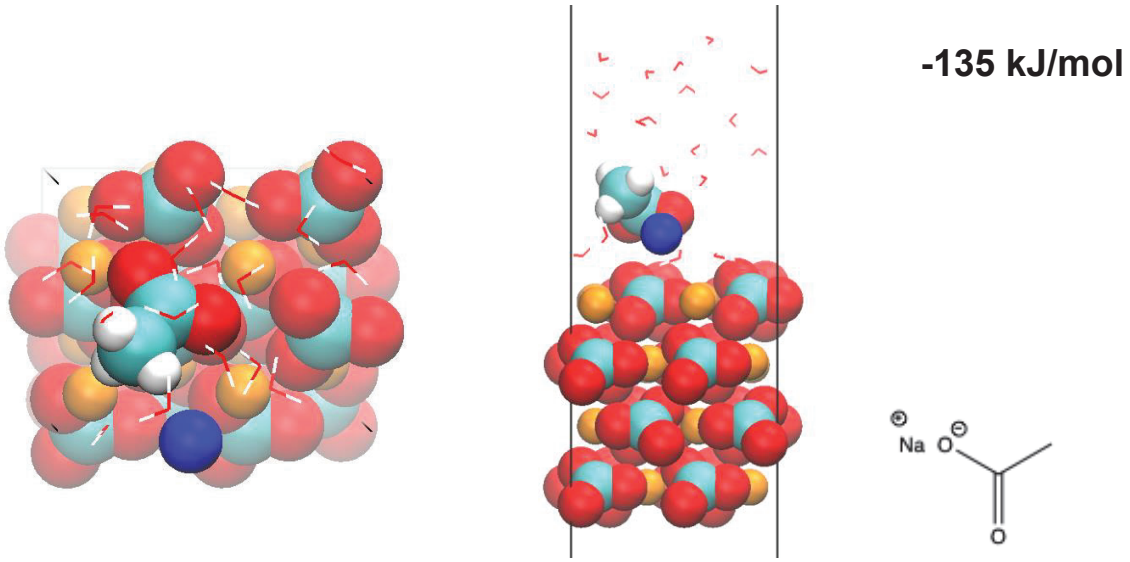

Figure 31. *Binding geometries for sodium acetate. One of the strongest interactions observed for magnesite was that of sodium acetate, where in both cases the sodium ion coordinates to the carbonate groups on the surface. The carboxyl group on sodium acetate coordinates to diagonal Mg atoms in a Mg...O-C-O...Mg fashion. The strong binding is due to a chelating effect of the carboxyl functional group on the metal ions in the magnesite (10.4) surface.*

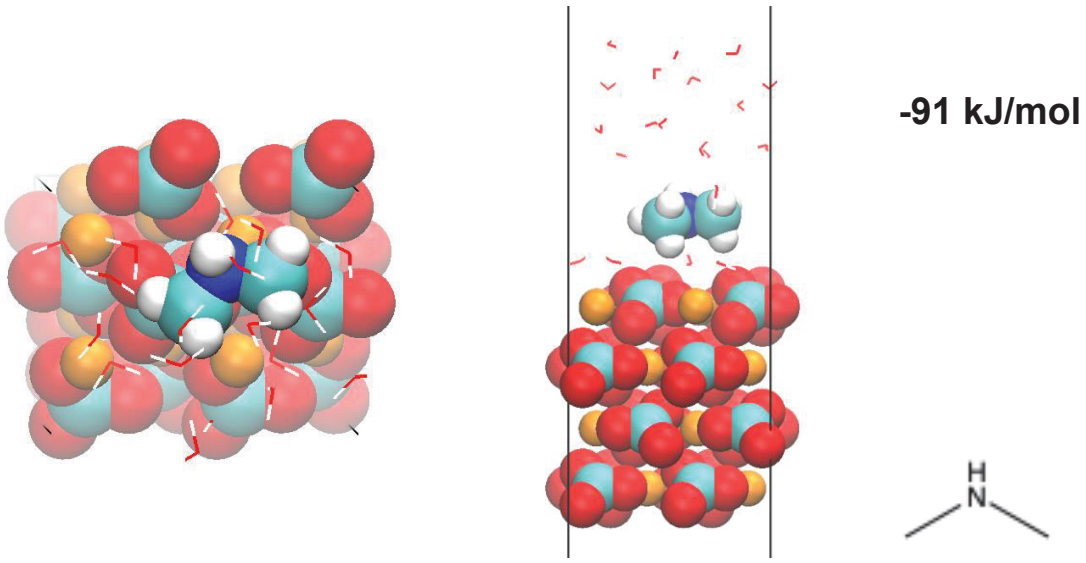

Figure 32. *Binding geometries for dimethylamine.* The main interaction of interest is the electronegative N interaction with the metal ions on the surface.

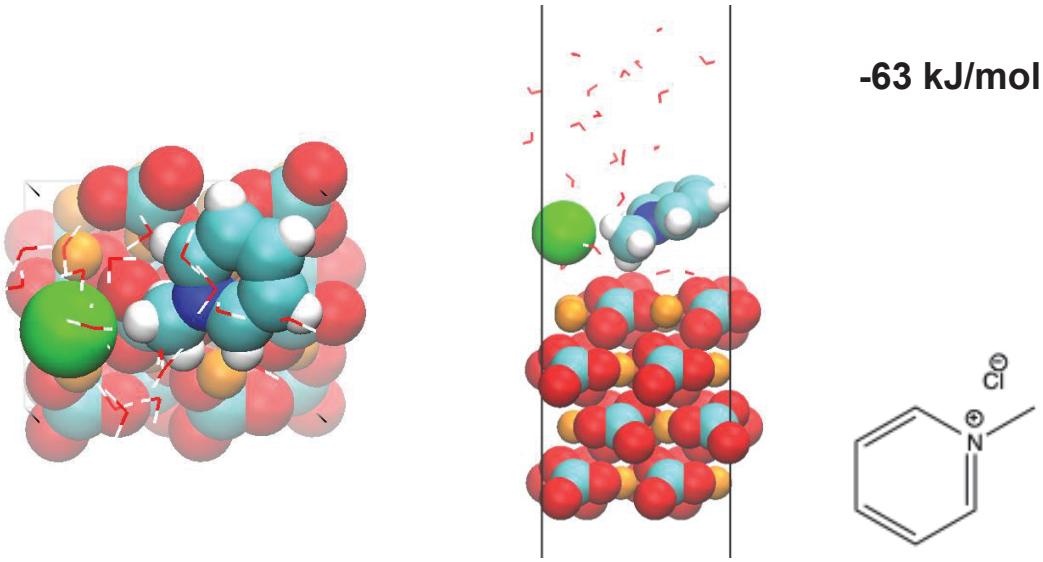

Figure 33. *Binding geometries for 1-Methylpyridinium chloride. The plane of the pyridinium ring relaxes to ~45° to the plane of the surface with the N-methyl group closest to the surface. The* H_{methyl} *atoms interact closely with the carbonate oxygens on the surface, and the chloride ion is solvated by concurrent interactions with water above the first water layer.*

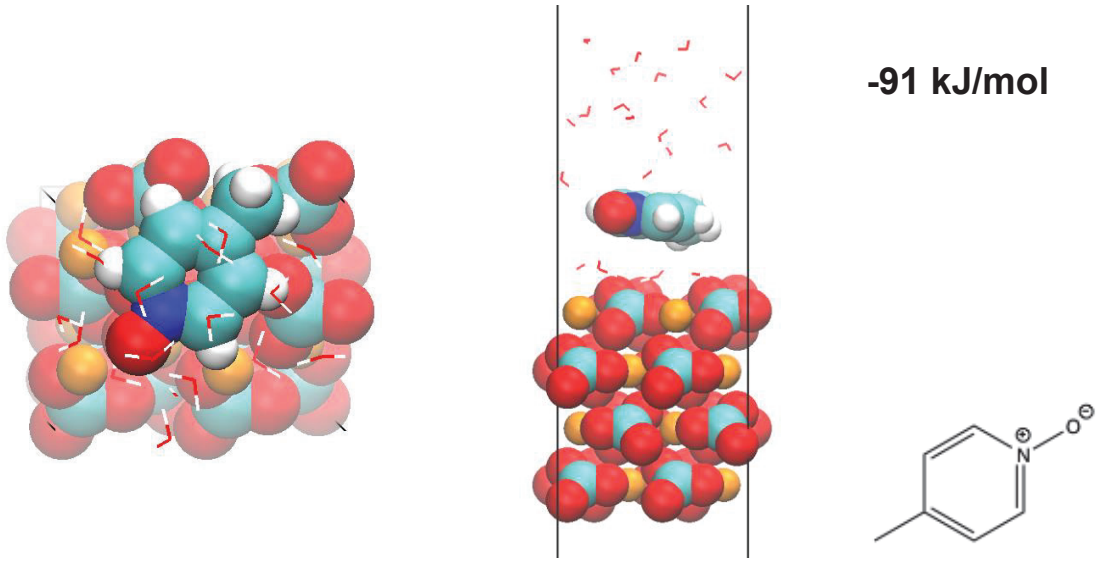

Figure 34. *Binding geometries for 4-Methylpyridine N-oxide. The molecule does not penetrate the first water layer. The plane of the ring is ~45° to the plane of the surface. The oxygen aligns directly to a single metal ion, adopting a planar configuration where the ring's plane is parallel with the surface.*

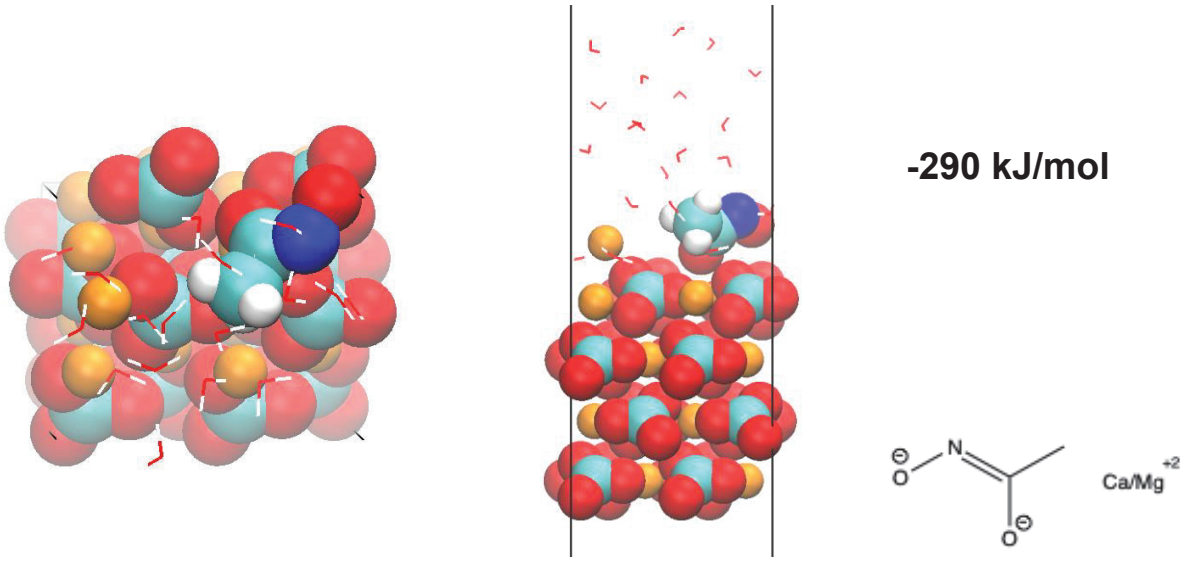

Figure 35. *Binding geometries for magnesium acetohydroxamate. The chief interaction is the electrostatic attraction of the anionic oxygen atoms to the surface metal ions. In the magnesite case the binding is direct on a single oxygen atom as O...Mg.*

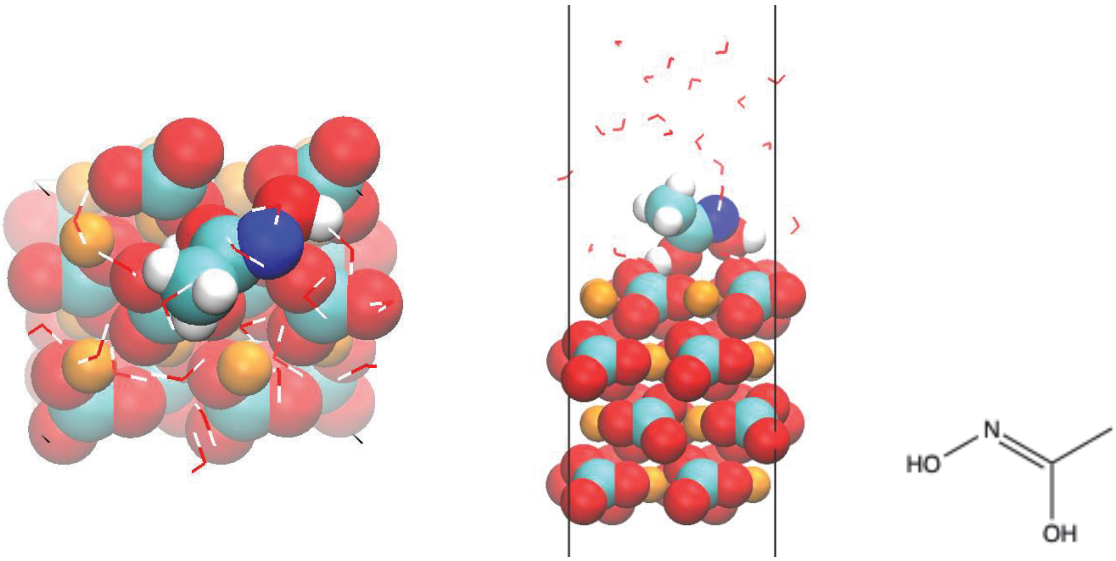

Figure 36. *Binding geometries for acetohydroxamic acid. A chelation effect evident as O...Mg...O. The angles of the O—H bonds of acetohydroxamic acid in the magnesite case are similar.*

Table 3. *Binding energy from periodic DFT-D calculations in this work. Again, (H_2O) denotes binding energy computed in solvated (aqueous) phase.*

#	Molecule	Magnesite 104 binding energy (kJ/mol)
1	1,3-Dimethylimidazolium chloride (aq)	-68.4
2	Sodium methylsulfate (aq)	-129
3	Sodium methylsulfonate (aq)	-100
4	Sodium acetate (aq)	-135
5	Dimethylamine (aq)	-90.6
6	1-Methylpyridinium chloride (aq)	-62.5
7	4-Methylpyridine *N*-oxide (aq)	-91.3
8	Magnesium acetohydroxamate (aq)	-290
9	Acetohydroxamic acid (aq)	-146

Toxicity and biodegradability.

PFOA and PFAS (perfluorinated surfactants currently in use in AFFF formulations) feature exceptionally poor biodegradability. The half-life of perfluorinated surfactants in the environment exceeds 50 years[61]. These materials remain in humans and other organisms unchanged for years. As a result, these compounds propagate through the food chain. PFOA and PFAS also feature moderate acute aquatic toxicity. LC_{50} (96 hours) of PFOA for Zebrafish has been reported around 119 mg/L.[62] LC_{50} of PFOS after 96 hours for marine microorganisms is around 131-176 mg/L, and >3.2 mg/L[63] for microalgae, and 9.1 mg/L for a freshwater fish species *Pimephales promelas*.

Biodegradability and toxicity of ionic liquids have been studied because of their role as green solvents in industrial applications. In particular, alkylimidazolium, alkylpyridinium, and other ionic liquids are immeasurably more biodegradable[64] than perfluorinated surfactants[61]. Both toxicity and biodegradability of 1-alkyl-3-methyl imidazolium and 1-alkyl-pyridinium ionic liquids[64, 65] increases with the alkyl chain length[64]. Zebra fish LC_{50} (96 hours) for 1-octyl-3-methyl imidazolium chloride is 150 mg/L[66]. Another source[67] reports a very different value of 48 mg/L for Zebrafish LC_{50} (96 hours) for 1-octyl-3-methtyl imidazolium chloride. The same source also reports Zebrafish LC_{50} (96 hours) for 1-butyl-3-methyl imidazolium chloride (897 mg/L). Guppy fish LC_{50} (96 hours) for 1-dodecylpyridinium bromide, 1-dodecyl-3-methylpyridinium bromide, and 1-dodecyl-4-methylpyridinium bromide are in the range 80-93 mg/L [65]. The value for 1-decyl-3-methylpyridinium bromide is 427 mg/L.

Estimated acute aquatic toxicity of our prototype for certain species is higher than the threshold values specified in MIL-F-24385F[1] (LC_{50}(96 hours) of 500 mg/L for Type 3), but our LC_{50}(96 hours) are based on literature for fish species other than Killiefish requested in MIL-F-24385F[1]. An estimated level of aquatic toxicity of our prototype containing sodium dodecylsulfate and 1-dodecyl pyridinium chloride (Type 3 formulation) is around 450-470 mg/L, which is almost at the threshold outlined in MIL-F-24385F[1]. Magnesium carbonate is a non-toxic compound.

Because of their low vapor pressure, ILs also pose low risk for environmental contamination and human inhalation both during and after fire extinguishment. The vapor pressure should decrease with alkyl chain length as our molecular dynamics simulations indicate. Thus, toxicity to humans associated with inhalation of long-chain ionic liquids should be negligible.

It is essential to realize that ionic liquids are immeasurably more biodegradable (in a matter of weeks) than perfluorinated surfactants that persist in the environment for decades although some long-chain ionic liquids may exhibit acute toxicity for some aquatic organisms comparable to that of perfluorinated surfactants. As a result, ionic liquids would not significantly propagate in the food chain, and their impact on the environment would be localized and short-term. On balance, the benefits of favorable biodegradability[64] would outweigh their slight aquatic toxicity[61]. Furthermore, there is a potential in the ionic liquid universe for the reduction of the toxicity and further enhancement of biodegradability. The latter is not the case for the current AFFF formulations that rely on perfluorinated surfactants.

Conclusions and Implications for Future Research

We have developed a successful AFFF prototype based on nano-encapsulated ionic liquids. We have shown using electron spray ionization mass spectrometry that ionic liquids are indeed bound to magnesium carbonate nanoparticles as intended. We also demonstrated that molecular dynamics simulations can successfully predict trends in interfacial tensions of ionic liquids. Density functional theory can help to rank different types of functional groups with respect to their ability to bind to magnesium carbonate surfaces and form NEIL.

Our fluorine-free AFFF prototype formulation meets the key requirements of MIL-F-24385F[1]. First, the spreading coefficient of our formulation is **3.32 mN/m**, which is above the required minimum threshold of 3 mN/m. Second, our formulation produces a stable foam with an estimated 25 % drainage time of **3.9** min. The latter is above the minimum threshold of 2.5 minutes. Third, we have shown that our prototype can extinguish small-scale hydrocarbon fires, although we did not perform full-scale fire tests in this phase. Fourth, all components in our prototype are biodegradable, unlike perfluorinated surfactants, which are currently used in AFFF formulations. Estimated acute aquatic toxicity of alkylpyridinium-based formulations is near the threshold values specified in MIL-F-24385F[1], but our LC_{50}(96 hours) are based on literature for fish species other than Killiefish requested in MIL-F-24385F[1].

In our future work, we will consolidate our work and further improve the performance of the developed formulation. We will work towards decreasing the toxicity of the developed foam formulation. This will be achieved by introducing polar groups in the alkyl chains or a change in head groups of ionic liquids. The initial screening effort can be accomplished with computational chemistry screening tools, which can be used to predict both toxicity and interfacial properties. Successful formulations identified in *in silico* screening can be further examined experimentally. The costs of *in silico* materials design efforts are significantly lower than those for actual experiments. In this phase, we did not attempt to optimize refractive index, viscosity, pH, and corrosion rate, but we plan to address these factors in the next phase by adding components that do not impact the firefighting performance.

References

1. Interim Amendment 3 of MIL-F-24385F: https://quicksearch.dla.mil/qsDocDetails.aspx?ident_number=283209.
2. Gipe, R.; Peterson, H. *Proportioning characteristics of aqueous film-forming foam concentrates*; NAVAL RESEARCH LAB WASHINGTON DC: 1972.
3. Oresky, S.; DeYoung, D., *The little book of big achievements*. Naval Research Laboratory: 2000.
4. Carn, F.; Colin, A.; Pitois, O.; Backov, R., Foam drainage study during plateau border mineralisation. *Soft Matter* **2012,** *8* (1), 61-65.
5. Gonzenbach, U. T.; Studart, A. R.; Tervoort, E.; Gauckler, L. J., Ultrastable particle-stabilized foams. *Angewandte Chemie International Edition* **2006,** *45* (21), 3526-3530.

6. Chevallier, E.; Monteux, C.; Lequeux, F.; Tribet, C., Photofoams: remote control of foam destabilization by exposure to light using an azobenzene surfactant. *Langmuir* **2012,** *28* (5), 2308-2312.
7. Petkova, R.; Tcholakova, S.; Denkov, N., Foaming and foam stability for mixed polymer–surfactant solutions: effects of surfactant type and polymer charge. *Langmuir* **2012,** *28* (11), 4996-5009.
8. Engelhardt, K.; Rumpel, A.; Walter, J.; Dombrowski, J.; Kulozik, U.; Braunschweig, B. r.; Peukert, W., Protein adsorption at the electrified air–water interface: implications on foam stability. *Langmuir* **2012,** *28* (20), 7780-7787.
9. Sham, A. Y.; Notley, S. M., Foam stabilisation using surfactant exfoliated graphene. *Journal of colloid and interface science* **2016,** *469*, 196-204.
10. Huang, Y.; Wencheng, Z.; Dai, X.; Zhao, Y., Study on water-based fire extinguishing agent formulations and properties. *Procedia Engineering* **2012,** *45*, 649-654.
11. Jho, C., Spreading of aqueous solutions of a mixture of fluoro-and hydrocarbon surfactants on liquid hydrocarbon substrates. *Journal of colloid and interface science* **1987,** *117* (1), 139-148.
12. Place, B. J.; Field, J. A., Identification of novel fluorochemicals in aqueous film-forming foams used by the US military. *Environmental science & technology* **2012,** *46* (13), 7120-7127.
13. Dlugogorski, B.; Kennedy, E.; Schaefer, T.; Vitali, J., What properties matter in fire-fighting foams? *SCIENCE, TECHNOLOGY AND STANDARDS FOR FIRE SUPPRESSION SYSTEMS.* **2002**, 57-76.
14. Renner, R., Growing concern over perfluorinated chemicals. ACS Publications: 2001.
15. Sheinson, R. S.; Williams, B. A.; Green, C.; Fleming, J. W.; Anleitner, R.; Ayers, S.; Maranghides, A.; Barylski, D., *The future of aqueous film forming foam (AFFF): performance parameters and requirements*. Naval Research Laboratory: 2002.
16. Hinnant, K. M.; Conroy, M. W.; Ananth, R., Influence of fuel on foam degradation for fluorinated and fluorine-free foams. *Colloids and Surfaces A: Physicochemical and Engineering Aspects* **2017,** *522*, 1-17.
17. Fameau, A.-L.; Saint-Jalmes, A., Non-aqueous foams: Current understanding on the formation and stability mechanisms. *Advances in colloid and interface science* **2017,** *247*, 454-464.
18. Smirnova, N.; Safonova, E., Ionic liquids as surfactants. *Russian Journal of Physical Chemistry A* **2010,** *84* (10), 1695-1704.
19. Benzagouta, M. S.; AlNashef, I. M.; Karnanda, W.; Al-Khidir, K., Ionic liquids as novel surfactants for potential use in enhanced oil recovery. *Korean Journal of Chemical Engineering* **2013,** *30* (11), 2108-2117.
20. Bera, A.; Belhaj, H., Ionic liquids as alternatives of surfactants in enhanced oil recovery—a state-of-the-art review. *Journal of Molecular Liquids* **2016,** *224*, 177-188.
21. Kilcrease, J. P.; Voelk, E., Liquid In-situ Transmission Electron Tomography Using Hitachi HILEM IL1000 TM Ionic Liquid. *Microscopy and Microanalysis* **2016,** *22* (S3), 810-811.
22. Hodyna, D.; Kovalishyn, V.; Rogalsky, S.; Blagodatnyi, V.; Petko, K.; Metelytsia, L., Antibacterial Activity of Imidazolium-Based Ionic Liquids Investigated by QSAR Modeling and Experimental Studies. *Chemical biology & drug design* **2016,** *88* (3), 422-433.

23. Neve, F.; Francescangeli, O.; Crispini, A.; Charmant, J., A2[MX4] Copper(II) Pyridinium Salts. From Ionic Liquids to Layered Solids to Liquid Crystals. *Chemistry of Materials* **2001,** *13* (6), 2032-2041.
24. Engin Özdil, S.; Akbaş, H.; Boz, M., Synthesis and Physicochemical Properties of Double-Chain Cationic Surfactants. *Journal of Chemical & Engineering Data* **2016,** *61* (1), 142-150.
25. Garg, P.; Kaur, G.; Chaudhary, G. R., Transition metal based single chained surfactants: synthesis, aggregation behavior and enhanced photoluminescence properties of fluorescein. *RSC Advances* **2016,** *6* (110), 108573-108582.
26. Gehlot, P. S.; Kulshrestha, A.; Bharmoria, P.; Damarla, K.; Chokshi, K.; Kumar, A., Surface-Active Ionic Liquid Cholinium Dodecylbenzenesulfonate: Self-Assembling Behavior and Interaction with Cellulase. *ACS Omega* **2017,** *2* (10), 7451-7460.
27. Qu, G.; Cheng, J.; Wei, J.; Yu, T.; Ding, W.; Luan, H., Synthesis, Characterization and Surface Properties of Series Sulfobetaine Surfactants. *Journal of Surfactants and Detergents* **2011,** *14* (1), 31-35.
28. Chang, T.; He, L.; Bian, L.; Han, H.; Yuan, M.; Gao, X., Brønsted acid-surfactant-combined catalyst for the Mannich reaction in water. *RSC Advances* **2014,** *4* (2), 727-731.
29. Rondla, R.; Lin, J. C. Y.; Yang, C. T.; Lin, I. J. B., Strong Tendency of Homeotropic Alignment and Anisotropic Lithium Ion Conductivity of Sulfonate Functionalized Zwitterionic Imidazolium Ionic Liquid Crystals. *Langmuir* **2013,** *29* (37), 11779-11785.
30. Lindner, J.-P., Imidazolium-Based Polymers via the Poly-Radziszewski Reaction. *Macromolecules* **2016,** *49* (6), 2046-2053.
31. Fang, C.; Kong, L.; Ge, Q.; Zhang, W.; Zhou, X.; Zhang, L.; Wang, X., Antibacterial activities of N-alkyl imidazolium-based poly (ionic liquid) nanoparticles. *Polymer Chemistry* **2019,** *10* (2), 209-218.
32. Merlet, C.; Salanne, M.; Rotenberg, B.; Madden, P. A., Imidazolium Ionic Liquid Interfaces with Vapor and Graphite: Interfacial Tension and Capacitance from Coarse-Grained Molecular Simulations. *The Journal of Physical Chemistry C* **2011,** *115* (33), 16613-16618.
33. Dominguez, H.; Berkowitz, M. L., Computer simulations of sodium dodecyl sulfate at liquid/liquid and liquid/vapor interfaces. *Journal of Physical Chemistry B* **2000,** *104* (22), 5302-5308.
34. Smit, B.; Schlijper, A. G.; Rupert, L. A. M.; Vanos, N. M., EFFECTS OF CHAIN-LENGTH OF SURFACTANTS ON THE INTERFACIAL-TENSION - MOLECULAR-DYNAMICS SIMULATIONS AND EXPERIMENTS. *Journal of Physical Chemistry* **1990,** *94* (18), 6933-6935.
35. Shinoda, W.; DeVane, R.; Klein, M. L., Coarse-grained molecular modeling of non-ionic surfactant self-assembly. *Soft Matter* **2008,** *4* (12), 2454-2462.
36. Rekvig, L.; Kranenburg, M.; Vreede, J.; Hafskjold, B.; Smit, B., Investigation of surfactant efficiency using dissipative particle dynamics. *Langmuir* **2003,** *19* (20), 8195-8205.
37. Vu, T. V.; Papavassiliou, D. V., Oil-water interfaces with surfactants: A systematic approach to determine coarse-grained model parameters. *Journal of Chemical Physics* **2018,** *148* (20).
38. Paredes, R.; Farnias-Sanchez, A. I.; Medina-Rodriguez, B.; Samaniego, S.; Aray, Y.; Alvarez, L. J., Dynamics of Surfactant Clustering at Interfaces and Its Influence on the Interfacial Tension: Atomistic Simulation of a Sodium Hexadecane-Benzene Sulfonate-Tetradecane-Water System. *Langmuir* **2018,** *34* (9), 3146-3157.

39. Ndao, M.; Goujon, F.; Ghoufi, A.; Malfreyt, P., Coarse-grained modeling of the oil-water-surfactant interface through the local definition of the pressure tensor and interfacial tension. *Theoretical Chemistry Accounts* **2017,** *136* (1).
40. Creton, B.; Nieto-Draghi, C.; Pannacci, N., Prediction of Surfactants' Properties using Multiscale Molecular Modeling Tools: A Review. *Oil Gas Sci. Technol. – Rev. IFP Energies nouvelles* **2012,** *67* (6), 969-982.
41. Wang, J.; Wolf, R. M.; Caldwell, J. W.; Kollman, P. A.; Case, D. A., Development and testing of a general amber force field. *J Comput Chem* **2004,** *25* (9), 1157-74.
42. Caleman, C.; van Maaren, P. J.; Hong, M.; Hub, J. S.; Costa, L. T.; van der Spoel, D., Force Field Benchmark of Organic Liquids: Density, Enthalpy of Vaporization, Heat Capacities, Surface Tension, Isothermal Compressibility, Volumetric Expansion Coefficient, and Dielectric Constant. *Journal of Chemical Theory and Computation* **2012,** *8* (1), 61-74.
43. Sprenger, K. G.; Jaeger, V. W.; Pfaendtner, J., The General AMBER Force Field (GAFF) Can Accurately Predict Thermodynamic and Transport Properties of Many Ionic Liquids. *The Journal of Physical Chemistry B* **2015,** *119* (18), 5882-5895.
44. Abascal, J. L. F.; Vega, C., A general purpose model for the condensed phases of water: TIP4P/2005. *The Journal of Chemical Physics* **2005,** *123* (23), 234505.
45. Vega, C.; de Miguel, E., Surface tension of the most popular models of water by using the test-area simulation method. *The Journal of Chemical Physics* **2007,** *126* (15), 154707.
46. Li, P.; Song, L. F.; Merz, K. M., Systematic Parameterization of Monovalent Ions Employing the Nonbonded Model. *Journal of Chemical Theory and Computation* **2015,** *11* (4), 1645-1657.
47. Li, P.; Roberts, B. P.; Chakravorty, D. K.; Merz, K. M., Jr., Rational Design of Particle Mesh Ewald Compatible Lennard-Jones Parameters for +2 Metal Cations in Explicit Solvent. *J Chem Theory Comput* **2013,** *9* (6), 2733-2748.
48. Martínez, L.; Andrade, R.; Birgin, E. G.; Martínez, J. M., PACKMOL: A package for building initial configurations for molecular dynamics simulations. *Journal of Computational Chemistry* **2009,** *30* (13), 2157-2164.
49. Zolotoyabko, E.; Caspi, E. N.; Fieramosca, J. S.; Von Dreele, R. B.; Marin, F.; Mor, G.; Addadi, L.; Weiner, S.; Politi, Y., Differences between Bond Lengths in Biogenic and Geological Calcite. *Crystal Growth & Design* **2010,** *10* (3), 1207-1214.
50. Maslen, E. N.; Streltsov, V. A.; Streltsova, N. R.; Ishizawa, N., Electron density and optical anisotropy in rhombohedral carbonates. III. Synchrotron X-ray studies of CaCO3, MgCO3 and MnCO3. *Acta Crystallographica Section B* **1995,** *51* (6), 929-939.
51. Leeuw, N. H. d.; Parker, S. C.; Rao, K. H., Modeling the Competitive Adsorption of Water and Methanoic Acid on Calcite and Fluorite Surfaces. *Langmuir* **1998,** *14* (20), 5900.
52. De Leeuw, N. H., Surface structures, stabilities and growth of magnesian calcites: A computational investigation from the perspective of dolomite formation. *American Mineralogist* **2002**, p 679.
53. CP2K: https://www.cp2k.org/.
54. Girifalco, L. A.; Good, R. J., A Theory for the Estimation of Surface and Interfacial Energies. I. Derivation and Application to Interfacial Tension. *The Journal of Physical Chemistry* **1957,** *61* (7), 904-909.
55. Hill, C.; Czajka, A.; Hazell, G.; Grillo, I.; Rogers, S. E.; Skoda, M. W. A.; Joslin, N.; Payne, J.; Eastoe, J., Surface and bulk properties of surfactants used in fire-fighting. **2018,** *530*, 686-694.

56. Duffy, D. M.; Harding, J. H., Simulation of Organic Monolayers as Templates for the Nucleation of Calcite Crystals. *Langmuir* **2004,** *20* (18), 7630-7636.
57. de Leeuw, N. H.; Cooper, T. G., A Computer Modeling Study of the Inhibiting Effect of Organic Adsorbates on Calcite Crystal Growth. *Crystal Growth & Design* **2004,** *4* (1), 123-133.
58. Freeman, C. L.; Asteriadis, I.; Yang, M.; Harding, J. H., Interactions of Organic Molecules with Calcite and Magnesite Surfaces. *The Journal of Physical Chemistry C* **2009,** *113* (9), 3666-3673.
59. Ataman, E.; Andersson, M. P.; Ceccato, M.; Bovet, N.; Stipp, S. L. S., Functional Group Adsorption on Calcite: I. Oxygen Containing and Nonpolar Organic Molecules. *The Journal of Physical Chemistry C* **2016,** *120* (30), 16586-16596.
60. Thomas, M. M.; Clouse, J. A.; Longo, J. M., Adsorption of organic compounds on carbonate minerals: 1. Model compounds and their influence on mineral wettability. *Chemical Geology* **1993,** *109* (1), 201-213.
61. Washington, J. W.; Jenkins, T. M., Abiotic Hydrolysis of Fluorotelomer-Based Polymers as a Source of Perfluorocarboxylates at the Global Scale. *Environmental Science & Technology* **2015,** *49* (24), 14129-14135.
62. Zhao, W. C.; Li, Q.; Xiao, F.; Song, G. L.; Lu, Y.; Yang, H. B.; Liao, C. X. In *The study of acute toxicity of perfluorooctanoic acid on Zebra fish*, Architectural, energy and information engineering: Proceedings of the 2015 International Conference on Architectural, Energy and Information Engineering (AEIE 2015), Xiamen, China, 2015; p 139.
63. Giesy, J. P.; Naile, J. E.; Khim, J. S.; Jones, P. D.; Newsted, J. L.; Whitacre, D. M., Aquatic Toxicology of Perfluorinated Chemicals. Springer New York: New York, NY, 2010; pp 1-52.
64. Amde, M.; Liu, J. F.; Pang, L., Environmental Application, Fate, Effects, and Concerns of Ionic Liquids: A Review. *Environmental Science & Technology* **2015,** *49* (21), 12611-12627.
65. Hafez, N. F. M.; Mutalib, M. I. A.; Bustam, M. A. B.; El-Harbawi, M.; Leveque, J. M., Ecotoxicity of Pyridinium Based ILs Towards Guppy Fish and Four Bacterial Strains. *Proceeding of 4th International Conference on Process Engineering and Advanced Materials (Icpeam 2016)* **2016,** *148*, 830-838.
66. Liu, T.; Guo, Y. Y.; Wang, J. H.; Wang, J.; Zhu, L. S.; Zhang, J.; Zhang, C., Assessing toxic effects of Omim Cl and Omim BF4 in zebrafish adults using a biomarker approach. *Environmental Science and Pollution Research* **2016,** *23* (8), 7360-7368.
67. Zhang, C.; Du, Z. K.; Wang, J. H.; Wang, J.; Zhou, T. T.; Li, B.; Zhu, L. S.; Li, W. X.; Hou, K. X., Exposed zebrafish (Danio rerio) to imidazolium-based ionic liquids with different anions and alkyl-chain lengths. *Chemosphere* **2018,** *203*, 381-386.
68. Bondi, C. A.; Marks, J. L.; Wroblewski, L. B.; Raatikainen, H. S.; Lenox, S. R.; Gebhardt, K. E., Human and Environmental Toxicity of Sodium Lauryl Sulfate (SLS): Evidence for Safe Use in Household Cleaning Products. *Environmental health insights* **2015,** *9*, 27-32.